doi.org/10.36721/PJPS.2026.39.5.REG.14029.1

An integrated strategy including chemical profiling, network pharmacology and experimental evaluation was used to investigate the effects of *Rubia yunnanensis* water decoction on vascular dementia

Jianghao Cheng, Chao Zhang, Liping Yang, Gaoyizhou Li, Xiaoli Jiang, Pu Chen and Xiaohua Duan*

Yunnan Key Laboratory of Dai and Yi Medicines, Yunnan University of Chinese Medicine, Kunming, Yunnan, P.R. China

Abstract: **Background**: Vascular dementia (VaD) is the second most prevalent cause of dementia following Alzheimer's disease. *Rubia yunnanensis*, a medicinal plant recorded in the Chinese Materia Medica, has historically been utilized for managing cerebral ischaemia-related disorders. While recent attention has focused on its neuroprotective potential, the specific mechanisms underlying the effects of *Rubia yunnanensis* water decoction (RY-W) on VaD remain unelucidated. **Objectives**: This study aimed to identify the active chemical components and elucidate the molecular mechanisms of RY-W in the treatment of VaD by integrating network pharmacology with experimental validation. **Methods**: The chemical constituents of RY-W and their potential therapeutic targets were analyzed using UPLC-MS/MS and network pharmacology techniques. To validate these findings, the cerebral protective effects of RY-W were assessed in a rat model of VaD. Cognitive function was evaluated using the Morris Water Maze (MWM) test. Pathological changes and molecular markers were analyzed via Hematoxylin and Eosin (HE) staining, Nissl staining, TUNEL fluorescence staining, Immunohistochemistry (IHC), and Western blotting. **Results**: Network pharmacology analysis identified IL-6, IL-1β, ALB, TNF, and AKT1 as potential core targets for RY-W. Experimental results demonstrated that RY-W significantly alleviated cognitive deficits in VaD rats. Furthermore, RY-W exhibited anti-inflammatory properties and reduced neuronal apoptosis. These neuroprotective effects appear to be mediated through the regulation of ALB and the PI3K-Akt signaling pathway. **Conclusion**: RY-W effectively ameliorates VaD pathology by exerting anti-inflammatory and anti-apoptotic effects. These findings highlight the involvement of ALB and the PI3K-Akt signaling pathway in the therapeutic action of RY-W, supporting its potential as a treatment for vascular dementia.

Keywords: Molecular docking; Network pharmacology; PI3K-Akt signaling pathway; *Rubia yunnanensis*; Vascular dementia

Submitted on 08-06-2024 – Revised on 24-10-2025 – Accepted on 07-11-2025

INTRODUCTION

Vascular dementia (VaD) is a prevalent form of dementia that ranks second to Alzheimer's disease in terms of the percentage of older patients affected. It accounts for roughly 20% of all dementia cases (Morgan & Mc Auley, 2024). Dementia is a medical condition marked by a decline in cognitive function, particularly in higher brain activity. The primary causes of this condition are cerebrovascular factors, including acute and chronic ischemia and hemorrhage of the cerebrovascular system (Skrobot *et al*., 2018). According to estimates, the population of individuals with dementia is projected to increase nearly thrice from the present 57.4 million to 153 million by 2025 (Collaborators, 2022). Patients with VaD are estimated to have a shorter time to confirmed survival (3.2 ± 1.4 years) than patients with Alzheimer's disease (5.8 ± 2.0 years), frontotemporal lobar degeneration (4.9 ± 2.2 years) and Lewy body dementia (4.7 ± 1.8 years) (Liang *et al*., 2021). The fundamental approach to preventing and treating VaD is generally considered to be the prevention of platelet aggregation, lipid accumulation, hypertension, diabetes and other related risk factors, in addition to the early treatment of cerebrovascular disease; however, the drugs currently used in clinical practice can only improve the symptoms of VaD and do not halt or decelerate the advancement of the disease (Yin *et al*., 2022). Hence, the creation of potent medications for the management of VaD is forthcoming.

Chronic cerebral ischemia (CCI) serves as the underlying pathophysiological foundation for various neurodegenerative disorders such as VaD, Binswanger's disease and Alzheimer's disease. It refers to chronic cerebral hypoperfusion due to various causes. Chronic cerebral hypoperfusion is one of the main pathological factors of VaD as it triggers neuroinflammation and neuronal apoptosis in the brain, leading to cognitive impairment (Mracsko *et al*., 2010). Research has demonstrated that correcting chronic cerebral hypoperfusion leads to enhanced cognitive function in a rat model of dementia (Fan and Roman, 2021; T. Li *et al*., 2022). The main pathological mechanisms of CCI include neuroinflammation, neuronal apoptosis, damage to the blood–brain barrier and oxidative stress-related damage,

**Corresponding author:* e-mail: 1047896527@qq.com

which in turn leads to neurotransmitter deficits in the central monoaminergic and cholinergic systems in addition to abnormalities in synaptic information transmission pathways (H. Yang *et al*., 2020; Yin *et al*., 2022).

As a multi-component, multi-targeted, green natural medicine, TCM has been increasingly accepted worldwide in recent years due to its effectiveness in treating various diseases including cancer, diabetes, new coronary viruses and VaD (An *et al*., 2021; Wang *et al*., 2020; Xiang *et al*., 2019). Previous studies have indicated that traditional Chinese medicines (TCMs), such as succinum and ginkgo biloba, have potential efficacy in VaD, not only by improving symptoms and enhancing quality of daily life for patients with VaD but also by slowing the disease progression and reducing related complications (Wei *et al*., 2022). Yunnan *Rubia yunnanensis* consists of the baked rhizome as well as roots from *Rubia yunnanensis* diels in their family *Rubiaceae*. It has the functions of activating blood and relaxing tendons, eliminating blood stasis and generating new blood, regulating qi and the blood, as well as the pharmacological effects of anti-thrombosis, anti-ischemia and anti-oxidation. Renowned Chinese physicians, including Chao Zhang, a distinguished TCM practitioner in Yunnan, frequently employ *Rubia yunnanensis* to address symptoms such as vertigo, sleeplessness, anemia and other conditions associated with inadequate blood circulation in the brain. *Rubia yunnanensis* is frequently employed by certain traditional healers to alleviate symptoms of vertigo and anemia. This traditional use suggests that *Rubia yunnanensis* (Yunnan origin) may have the potential to treat CCI-induced vascular dementia. Anemia has also been reported to correlate with the risk of dementia by as much as 56% and low hemoglobin concentrations are predictive of cognitive impairment in older adults (Qiang *et al*., 2023). Furthermore, we previously reported that the alcoholic extract of *Rubia yunnanensis* also plays a promising role in inhibiting oxygen–glucose deprivation/reperfusion (OGD/R)-induced neuron death (Cheng *et al*., 2024); however, whether *Rubia yunnanensis* water decoction (RY-W) can be used to treat CCI-induced VaD is unknown.

Network pharmacology rooted in systems biology that examines the intricate networks connecting drug chemical components, gene targets and disease multiplexes. By doing so, it can anticipate the physiological processes and signaling pathways implicated inside its treatment of a disease with a drug (Liang *et al*., 2014). This study employed the chemical profiling approach to evaluate the chemical components of RY-W. Additionally, we utilized the network pharmacology method to establish the "drug-component-target-pathway-disease" (D-C-T-P-D) network of RY-W in treating of VaD. To systematically map biological processes and associated pathways, functional annotation was performed through Gene Ontology (GO) term classification and Kyoto Encyclopedia of Genes and Genomes (KEGG) pathway enrichment. Computational molecular docking simulations were subsequently conducted to assess ligand-target interactions between bioactive compounds and critical protein targets. Notably, our multi-platform analytical strategy synergistically combined topological relationships from the D-C-T-P-D network, functional enrichment profiles from GO/KEGG platforms and three-dimensional binding conformation analyses. This integrated approach revealed two potential mediators of RY-W's pharmacological activity in VaD: the plasma transport protein albumin (ALB) demonstrated significant molecular interactions, while the PI3K/Akt signaling cascade emerged as a prominent regulatory pathway. For further validation, we conducted pharmacodynamic experiments using Sprague Dawley (SD) rats as experimental subjects, to create a rat model of VaD using the two-vessel occlusion (2VO) method. The pharmacodynamic impact of RY-W was confirmed using the Morris water maze (MWM) test, pathological staining, immunohistochemistry (IHC) and Western blotting (WB). In addition, we assessed whether the molecular mechanism is associated with the ALB and PI3K/Akt pathways in management of VaD.

The primary objective of this study was to examine whether RY-W could improve cognitive impairment in VaD rats and to assess the related molecular mechanisms, thus providing a research basis for further clarifying and expanding the clinical application of Yunnan *Rubia yunnanensis* in dementia. Fig. 1 shows the flow chart of our entire study.

MATERIALS AND METHODS

Chemicals and reagents

HPLC-grade methanol and acetonitrile were sourced from Merck KgaA (Darmstadt, Germany). HPLC-grade formic acid was purchased from Aladdin (Shanghai, China). *Rubia yunnanensis* (Y202305130010), authenticated by Prof. Zili Yin of Yunnan University of Chinese Medicine, was provided by Yunnan Huide Pharmaceutical Co., Ltd. (China). Antibodies against IL-6 (1:200, GB11117), IL-1β (1:500, GB11113) and ALB (1:1000, GB122080), along with 4% paraformaldehyde tissue fixative, were obtained from Wuhan Servicebio Technology Co., Ltd. (China). Isoflurane was purchased from Jiangsu Zhongmu Beikang Pharmaceutical Co., Ltd. Four-gauge absorbable polyglycolic acid (PGA) surgical thread was purchased from Shanghai Pudong Jinhuan Medical Products Co., Ltd.

Preparation of RY-W and standard solutions

In total, 400 g of Yi medicine *Rubia yunnanensis* powder was soaked 10 times the volume of water for 2 h, decocted and boiled for 30 mins. Eight times the water was added and decocting was performed again, followed by boiling for 30 mins. Decocting was then performed with six times

the volume of water and boiled for 30 mins. After three iterations of boiling a liquid to extract its soluble components, the resulting liquid produced by passing it through a sieve was combined and allowed to sit undisturbed for 24 hours at the ambient temperature. The supernatant was concentrated using a rotary evaporator to obtain a concentrated extract of 40.72 g, which was then stored at a temperature of -80 °C. Samples were extracted from the freezer set at a temperature of -80 °C, thawed and vortexed for 1 min or stirred manually with a weighing spoon for 30 sec if vortexing was not possible. The pre-cooled internal standard extract (70% methanol in water) was added to the sample at a ratio of 600 µL extractant per 50 mg sample (i.e., 12 µL/mg). The mixture was then vortexed for a duration of 15 minutes. Centrifugation (12000 revolutions per minute and a temperature of 4 °C) for a duration of 3 mins. The resulting liquid was then passed through a microporous filter membrane with a pore size of 0.22 µm. The filtered liquid was stored in an injection vial for further liquid chromatography (LC)–mass spectrometry (MS)/MS testing.

LC/MS equipment and parameters

Chromatographic separation was performed on an ExionLC™ AD UPLC system (SCIEX, USA) equipped with an Agilent SB-C18 column (1.8 µm, 2.1 × 100 mm). The chromatographic separation was achieved using a column thermostat maintained at 40°C coupled with a mobile phase delivery system operating at 0.35 mL/min. The binary solvent system comprised (A) 0.1% formic acid in ultrapure water and (B) 0.1% formic acid in acetonitrile, with the following optimized gradient profile: initial 5% B (0-0.1 min), linear ramp to 95% B over 8.9 min (0.1-9 min), isocratic maintenance at 95% B (9-10 min), rapid return to initial conditions (10-11.1 min), followed by a 2.9-minute column re-equilibration phase (11.1-14 min). Automated sample introduction employed a 2 µL injection volume for analytical consistency.

Mass spectrometric detection was performed on a Thermo Ultimate 3000LC Q Exactive HF platform (Thermo Fisher Scientific, USA) conFig.d with dual-polarity electrospray ionization (ESI). Critical ionization parameters included a source temperature of 550°C with spray voltages modulated between +5500 V (positive mode) and -4500 V (negative mode). Gas flow optimization established the following pressures: nebulizing gas (GSI) at 50 psi, auxiliary gas (GSII) at 60 psi and curtain gas (CUR) at 25 psi. For targeted compound analysis, the triple-quadrupole (QQQ) system operated in multiple reaction monitoring (MRM) mode using nitrogen-mediated collision-induced dissociation (medium CID setting). Individual MRM transitions underwent parameter optimization through systematic adjustment of declustering potential (DP) and collision energy (CE), while precursor/product ion pairs were selectively monitored based on chromatographic elution profiles to enhance analytical specificity.

Detector signals (counts per second, CPS) were recorded for quantification. Chromatographic data were processed using MultiQuant software for retention time alignment, peak detection and integration. Metabolic features were characterized via the MWDB (metware database) using secondary spectral data, excluding isotopic signals, adduct ions (K+, Na+, NH4+) and fragment ions from higher-molecular-weight compounds. Peak areas of identified compounds across samples were normalized for quantitative comparison (Fraga *et al*., 2010). To assess technical reproducibility, quality control (QC) samples-prepared from mixed extracts of all test samples-were analyzed successively after every 10 test samples.

Establishing the database of RY-W components

Initially, ultra-high performance liquid chromatography-mass spectrometry (UPLC-MS) identified chemical components in RY-W. Subsequently, these components were analyzed via TCMSP (https://old.tcmsp-e.com/tcmsp.ph) to screen active ones (oral bioavailability >30, drug-likeness >0.18) and via SwissDrugDesign's SWISSADME (http://www.swissadme.ch/) (high gastrointestinal absorption, ≥2 "YES" in Lipinski/Ghose/Veber/Egan/Muegge rules). Potential targets were predicted by SwissTargetPrediction (http://www.swisstargetprediction.ch/, probability >0.12), standardized to gene symbols via UniProt (https://www.uniprot.org/) and supplemented by SymMap (https://www.symmap.org/). Ultimately, PubChem (https://www.ncbi.nlm.nih.gov/pubmed/) and PharmMapper (https://lilab-ecust.cn/pharmmapper/) annotated component properties and verified targets.

Database establishment for VaD therapeutic targets

In order to find possible therapeutic targets for Vascular Dementia (VaD), we conducted a search across various databases using the specific search term "Vascular Dementia". We restricted the search results to include only information relating to the human species (Homo sapiens). The following databases were consulted: the DisGeNET database (https://www.disgenet.org/); SymMap (https://www.symmap.org/); TTD (https://db.idrblab.net/ttd/) and the GeneCards database (https://www.genecards.org/). Information on potential VaD-related therapeutic targets identified from the search of the above databases was taken and summarized into a list, along with the removal of duplicate entries, resulting in a final list of potential pharmacological targets for VaD.

Analysis of protein-protein interactions network

The possible pharmacological targets in VaD, as stated in section 2.5, were compared with the known or postulated targets of the chemical components of RY-W, as described in section 2.4, using the SRplot sharing tool available at https://www.bioinformatics.com.cn/. Intersecting targets that were common to both lists represented possible targets for RY-W therapy of VaD. The SRplot sharing features were utilized to create Venn diagrams. In order to clarify

the connections between the proteins found in this procedure, we generated their protein-protein interaction (PPI) networks using the STRING database (https://string-db.org/). The networks were produced, specified as "*Homo sapiens,*" and the confidence level was set to 0.400, which represents a medium degree of confidence. Topological property analysis was conducted via a network analyzer in Cytoscape 3.9.1 (Huang *et al*., 2023; Shannon *et al*., 2003), taking node degree, betweenness centrality and closeness centrality as core screening indicators. Core targets were screened in three steps: 1) Initial screening: Targets with node degree ≥ twice the network's mean degree (high association) were retained; 2) Refined screening: Cytoscape's cytoNCA plugin calculated betweenness/closeness centrality, retaining targets with all three indicators ≥ median; 3) Confirmation: Key candidates were ranked by node degree (descending), with top-ranked targets identified as core targets.

Pathway enrichment analysis based on GO and KEGG

The acquired core targets were imported into the Database for Annotation, Visualization and Integrated Discovery (DAVID) Version 6.8 for GO and KEGG pathway enrichment analysis, with the species specified as "*Homo sapiens*"(Huang da *et al*., 2009). The findings were organized based on the –log10 (*p*, adjust) values and all genes were used as the background for the enrichment analysis. Furthermore, the systematic data exhibited excellent timeliness and a threshold of $p < 0.05$ was employed to filter the significant biological processes and pathways of GO and KEGG.

Analysis and construction of network

In order to simplify the understanding of the intricate connection between the chemical makeup of RY-W and established treatment targets for VaD, a D–C–T–P–D interaction network was constructed using Cytoscape 3.9.1 software. This network provides a scientific explanation for the intricate connection between medications, components, targets and disorders. The analyzer plugin was utilized to examine the nodes of a network graph, offering a means to incorporate, scrutinize and depict data for intricate network investigations (Huang *et al*., 2019).

Molecular docking study of putative active RY-W components

Network topology analysis employing degree centrality identified six principal nodal proteins within the protein-protein interaction (PPI) network. To establish a computational validation protocol, five bioactive components of RY-W exhibiting maximal network connectivity metrics were systematically selected from the D–C–T–P–D pharmacological network. Structural refinement involved retrieving crystallographic coordinates of target proteins from the Protein Data Bank (PDB, https://www.rcsb.org/), complemented by acquisition of small molecule ligands from PubChem (https://pubchem.ncbi.nlm.nih.gov/). Moleculer preparation protocols included ligand structure conversion to Mol2 format through conformational optimization, enabling precise molecular docking simulations. Pymol 2.5.2 (https://pymol.org/2), AutoDockTools 1.5.6 (https://autodocksuite.scripps.edu/adt/) (Morris *et al*., 2009) and AutoDock Vina 1.2.0 (http://vina.scripps.edu/) (Trott & Olson, 2010) software were used for the dehydration, desolventization, hydrogenation and optimization of these core target proteins, which were stored in pdbqt format. Docking sites for various RY-W key active components on core target proteins were identified and a grid file was prepared. Molecular docking was performed using Autodock software to create a model containing the selected proteins and interacting RY-W key component substances with the selection of the optimal docking conformation. The binding energy was computed to assess the affinity of the major components of RY-W towards the core target protein. A binding energy threshold of ≤ -5.0 kcal/mol indicates favorable interactions, while ≤ -7.0 kcal/mol signifies strong binding affinity (Meli *et al*., 2021). The data were visualized using Pymol 2.5.2 and Discovery Studio 2020 Client (https://discover.3ds.com/discovery-studio-visualizer-download).

Molecular dynamics simulation

To further optimize the binding modes of protein-small molecule complexes, conventional molecular dynamics (MD) simulations were performed on the pair of complexes with the highest binding energy using the Desmond program. The OPLS2005 force field was utilized to parameterize proteins and small molecules and the TIP3P model was adopted to describe solvent water molecules. The protein-small molecule complexes were placed in cubic water boxes and solvated, followed by neutralizing the system charge by adding 0.150 M chloride ions (Cl^-) and sodium ions (Na^+). The system energy was minimized within 50,000 steps via the steepest descent method and then 50,000-step NVT (constant temperature) equilibration and 50,000-step NPT (constant temperature and pressure) equilibration were sequentially conducted, with the positions of heavy atoms restrained during the equilibration processes. The system temperature and pressure were maintained at 300 K and 1 bar, respectively. After the above two equilibration stages, unrestrained 100 ns MD simulations were carried out and the energy and coordinate data of trajectories were saved every 10 ps.

Animals and drug administration

65 male pathogen-free SD rats, 8 weeks old, 260 ± 20 g, were purchased from SPF (Beijing Biotechnology Co., Ltd.) and modeled after 1 week of isolation and domestication. Food and water were freely available at a temperature of 21 ± 2 ℃. The room was subjected to a 12-hour period of illumination from 6:00 to 18:00, followed by a 12-hour period of darkness from 18:00 to 6:00. Accepted all the stages involved in animal research for this project. Furthermore, this experiment adhered to the rules set forth by the National Institute for Animal Research.

Modeling of VaD

To establish the rat model of VaD, the previously reported 2VO method was used (Pan *et al*., 2021). The rats were involved in a 12-hour fasting period before surgery, while retaining unrestricted access to hydration. The rats were placed in a closed glass container and 3.5% isoflurane was passed through it. After the turning over reflex disappeared, the rats were moved to the operating table, fixed in the supine position and anesthesia was maintained by continuous inhalation of 1.5% isoflurane. The voluntary respiration of the rats was closely observed to avoid the lethal situation of anesthetic allergy or overdose. After anesthesia, they were fixed in the supine position on the surgical plate at a constant temperature of 37ºC, the neck area was clipped and the skin was prepared. After being fully sterilized with iodophor, the median skin of the rat's neck was cut with surgical scissors and an incision of approximately 1 cm was made. The subcutaneous tissue was bluntly separated and the common carotid artery was searched along both sides of the trachea, minimizing stimulation to the trachea and the vagus nerve, which was parallel to the common carotid artery, was gently detached with a glass parting needle. The common carotid artery was permanently tied off at both ends with a 4-gauge sterile surgical wire, completely blocking the blood flow. After surgery, the subcutaneous tissue and skin were sutured layer by layer with no. 4 absorbable PGA surgical thread and then fully sterilized with iodophor. Attention was paid to keeping the rats warm and observing their postoperative status; they were returned to the standard environment after awakening. Erythromycin ointment was applied externally to the neck incision of all operated rats to prevent infection for 3 days. In the sham operation (Sham group), the carotid artery was not ligated in rats and only surgical procedures (without ligation) were performed.

Model evaluation

Neurobehavioral scoring of the modeled rats was performed on postoperative day 3 to determine whether the modeling was successful or not, based on a modified five-point scale developed by (1989). A score of 1 to 3 was required for a successful model and scores of 0 and 4 were excluded as modeling failures.

Grouping and RY-W management

Sixty rats were randomly divided into four groups (n=15 per group): sham-operated (Sham), operated (2VO), RY-W low-dose (2VO+0.27g/kg RY-W) and RY-W high-dose (2VO+0.81g/kg RY-W). Treatments were administered via oral gavage (1 mL/100 g body weight) daily for 30 days, starting on postoperative day 3. The Sham and 2VO groups received 0.9% saline, while RY-W groups received corresponding drug solutions.

Test of MWM

After 30 days of medication treatment, the learning and memory abilities of rats were assessed using the MWM test, with 10 rats selected per group for behavioral evaluation. A cylindrical pool with a diameter of 150 cm and a height of 50 cm contained a round jumping platform that was 30 cm high and had a diameter of 10 cm. Water from the tap was used to fill the pool and the water temperature was set to 25 ± 0.5ºC. Ink was then placed in the water so that the animals could not see the jumping platform. The rats were placed in quadrant IV and entered the water from quadrant II, facing the tank wall. The average time it took for the rats to find and stay at the platform for 3 sec within 90 sec was taken as the average performance of the rats (escape latency). If the rats were unable to find the platform within the designated 90 sec timeframe, the platform was guided to them and remained there for 10 sec. The rats underwent bi-daily training sessions, rotating in a clockwise direction within a specific quadrant during each session. This training regimen was conducted for a period of 5 consecutive days in the Hidden platform test. On the sixth day, a probe test was conducted by removing the submerged platform and placing rats in quadrant II (opposite the original platform location), with their heads facing the pool wall. Rats were allowed to swim freely for 120 sec. The Supermaze System (Shanghai Xinruan Information Technology Co. Ltd., China) recorded platform-crossing frequency, as well as quadrant-specific swimming duration and speed within the original target area.

Histological and fluorescent staining analysis

Histological testing is critical for assessing nerve cell injury and drug effects. Six rats per group were used for HE and Nissl staining and 3 rats per group for TUNEL staining. Rats were anesthetized with 3.5% isoflurane, transcardially perfused with saline (250 mL) followed by 4% paraformaldehyde (100 mL) and brains were post-fixed in 4% paraformaldehyde for 48 hours. After paraffin embedding, 3-μm-thick coronal sections were prepared for staining. Remaining hippocampus tissue was snap-frozen in liquid nitrogen and stored at -80°C. For hematoxylin and eosin (HE) and Nissl staining, sections underwent xylene deparaffinization (5 min), gradient ethanol dehydration (70%, 95%, 100%; 5 min each) and staining with HE or toluidine blue. Histopathological changes were visualized using CaseViewer 2.4 software at 200× magnification.

TUNEL staining was conducted to evaluate apoptosis in the hippocampus. The sections were treated with 0.5% TritonX-100 in PBS for 5 minutes at room temperature and subsequently rinsed twice with PBS. Subsequently, a volume of 50 μL of TUNEL detection solution was introduced to the samples and subjected to incubation for a duration of 60 minutes at a temperature of 37 °C. The slices underwent three rounds of washing with PBS. The samples were blocked using an anti-fluorescence quenching solution, examined under a fluorescence microscope and quantitatively analyzed using ImageJ (NIH, Bethesda, MD).

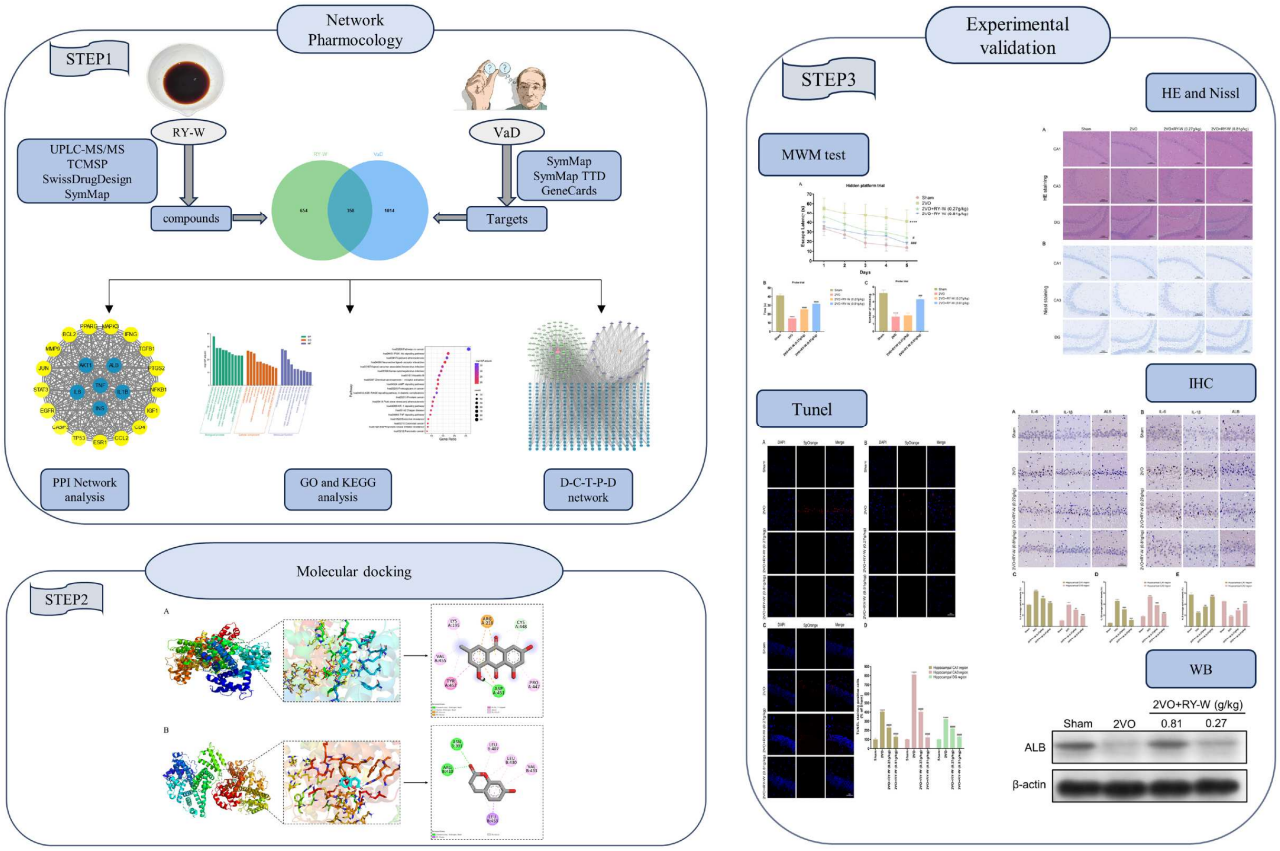

Fig. 1: Flow chart of the study protocol for the *Rubia yunnanensis* water decoction (RY-W) administration in vascular dementia (VaD).

IHC analysis

Three rats per group were selected and their brain slices fixed with 4% paraformaldehyde and embedded in paraffin were used-3 slices per rat-for IHC staining with antibodies against IL-6, IL-1β and ALB. The expression of IL-6, IL-1β and ALB in rat brain tissue was analyzed based on the average optical density (AOD) values of positive areas of brain tissue. Quantitative analysis was conducted using ImageJ software (NIH, Bethesda, MD).

Analysis of WB

Three rats per group were selected and their hippocampal tissues stored at –80 °C were lysed with RIPA lysis buffer (PSMF: RIPA lysate = 1:100; PMSF; cat. No. MFCD00007424; Amresco, Solon, OH, USA; RIPA; cat. No. P0013C; Beyotime Biotech Inc.) on ice for 30 min. The homogenized tissues underwent centrifugation at a speed of 12,000 rpm at a temperature of 4 °C for a duration of 10 minutes in order to eliminate debris. Supernatants were collected and protein concentrations were determined using a bicinchoninic acid (BCA) assay kit (Beyotime Biotech). Proteins were resolved via sodium dodecyl-sulfate polyacrylamide gel electrophoresis (SDS-PAGE) and transferred to 0.45 μm polyvinylidene fluoride (PVDF) membranes (cat. No. IPFL85R; Millipore). Membranes were blocked with 5% bovine serum albumin (BSA) for 2 hours at room temperature, followed by overnight incubation at 4°C with primary antibodies: anti-ALB (1:1000, GB122080; Wuhan Servicebio), anti-PI3K (1:1000, 4257), anti-p-PI3K (1:1000, 4228), anti-Akt (1:1000, 9272), anti-p-Akt (1:1000, 9271; all from Cell Signaling Technology) and anti-β-Actin (1:1000, ab8226; Abcam). Afterwards, it was treated with a secondary antibody [Goat Anti-Rabbit IgG Hirsl (HRP), diluted at a ratio of 1:10000; cat. Ab6721 is a rabbit antibody that specifically targets mouse IgG. It is labeled with horseradish peroxidase (HRP) and should be diluted at a ratio of 1:10000. The product is categorized as a hanger for use in experiments with mouse IgG. The sample was treated with Ab6728 from Abcam, located in Cambridge, UK and then kept at room temperature for a duration of 2 hours. The quantification of the peak regions of the bands was performed using an automated gel imaging equipment from Beijing, China and Image J software from NIH, Bethesda, MD. β-actin used as a reference. The ratio of 'target protein gray value/β-actin gray value' was calculated as the relative expression level of the target protein for subsequent statistical analysis.

Statistical analysis

Data were analyzed using GraphPad Prism 8.0 (GraphPad Software Inc., La Jolla, CA, USA) and expressed as mean

± standard error of the mean (SEM). Comparisons between two groups were performed using paired t -tests (normally distributed data). One-way ANOVA were applied for multiple-group comparisons, depending on data distribution. Two-way repeated-measures ANOVA was used for hidden platform trials and immunohistochemistry (IHC)/TUNEL analyses. Statistical thresholds were established with $p < 0.05$ denoting significance and $p < 0.01$ representing heightened significance.

RESULTS

Identifying chemical components present in RY-W

The UPLC-MS/MS technique was used to detect RY-W and optimize the chromatographic and mass spectrometric conditions. The RY-W components were identified according to the self-constructed database MWDB. Fig. 2 presents the overlaid Total Ion Chromatogram (TIC) of QC samples. The abscissa is retention time (RT) and ordinate is ion current intensity. Consistent retention times and peak intensities in the overlaid TIC confirmed stable mass spectrometry performance. The analysis revealed that RY-W consisted of a grand total of 1118 components. These components encompassed 121 amino acids and their derivatives, 167 phenolic acids, 53 nucleotides and their derivatives, 105 flavonoids, 45 quinones, 81 lignans and coumarins, one tannin, 113 alkaloids, 52 terpenoids, 70 organic acids, one steroid, 157 lipids and 152 other components. (Supplementary table 1).

Putative targets of the chemical components of RY-W

Specifically, 156 data entries were retained after screening via TCMSP, 17731 data entries were obtained through SwissTargetPrediction and merging and deduplicating these with 1236 data entries from SymMap yielded 154 active components of RY-W. The data were taken into a concatenation set and the duplicate values were removed to summarize the 1012 target information of the 154 active components in RY-W. The detailed one-to-one correspondence information of these components and targets is provided in Supplementary table 2.

Identified therapeutic targets for VaD

The database search yielded a grand total of 1509 targets associated to VaD. Out of these, 212 entries were found in the DisGeNET database, while the SymMap and TTD databases had no entries. However, the GeneCards database had a total of 1297 entries. After removing duplicate entries, we identified 1372 targets associated to VaD (see Supplementary table 3). The identified targets corresponded to the 1012 targets in RY-W. In conclusion, a grand total of 358 overlapping targets were successfully mapped using the SRplot sharing tool (Fig. 3A). Among the 154 active components of RY-W, emodin, choline, coumarin, catechin and 3-O-methyl quercetin respectively, corresponded to 83, 72, 72, 65 and 52 cross-targets between RY-W and VaD, indicating their importance in the treatment of VaD by RY-W.

PPI network construction and core targets selection

The intersecting target PPI network of RY-W and VaD consisted of 357 target nodes and 12376 lines, revealing the complex interconnections among these targets. The mean degree value was 69.3. The color and size of the targets were indicative of the degree value, with bigger values representing a stronger correlation among the nodes in the network (Fig. 3B). The top 10 targets in terms of degree value were used as important targets for the RY-W treatment of VaD (Fig. 3C, degree value size histogram). The first screening condition was greater than or equal to twice the median degree value (degree value ≥ 116) and 58 candidate targets were obtained. The median and proximity values of the candidate targets were obtained with the cytoNCA plug-in analysis and further screening was performed for targets greater than or equal to the median of the degree value, median value and proximity value. In total, 23 candidate targets were obtained (Fig. 3D). Among them, the top six core targets in terms of the selectivity value or as core targets of RY-W in the prevention and treatment of VaD were TNF, IL-6, ALB, AKT1, IL-1β and INS, with degree values of 248, 246, 238, 238, 234 and 232, respectively (see Supplementary Table 4 for degree information of the PPI network).

Analysis of functional and pathway enrichment using GO and KEGG

The biological features of the intersection targets between RY-W and VaD were investigated using GO and KEGG analysis, which also identified the signaling pathways involved. The GO analysis revealed 1326 enhanced biological processes, 165 cellular components and 249 molecular activities. The top 10 were selected for demonstration based on their corrected *p* values and are listed in Supplementary table 5. The GO category analysis revealed several biological processes, including the response to xenobiotic stimulus, negative regulation of apoptotic process, inflammatory response and response to lipopolysaccharide. The cellular components identified were neuronal cell body, dendrite, plasma membrane, membrane raft, extracellular region, extracellular space, cell surface and perinuclear region of the cytoplasm. The molecular functions revealed critical binding modalities encompassing enzyme binding, receptor binding and protein serine/threonine/tyrosine kinase activity, etc. (Fig. 4A).

The KEGG pathway enrichment analysis identified 193 significantly enriched signaling pathways (Supplementary table 6). The findings suggest that the therapeutic mechanisms of RY-W in treating VaD may involve a multidimensional molecular regulatory network. This network includes pathways associated with the PI3K-Akt signaling pathway, lipids and atherosclerosis, as well as the TNF signaling pathway (Fig. 4B).

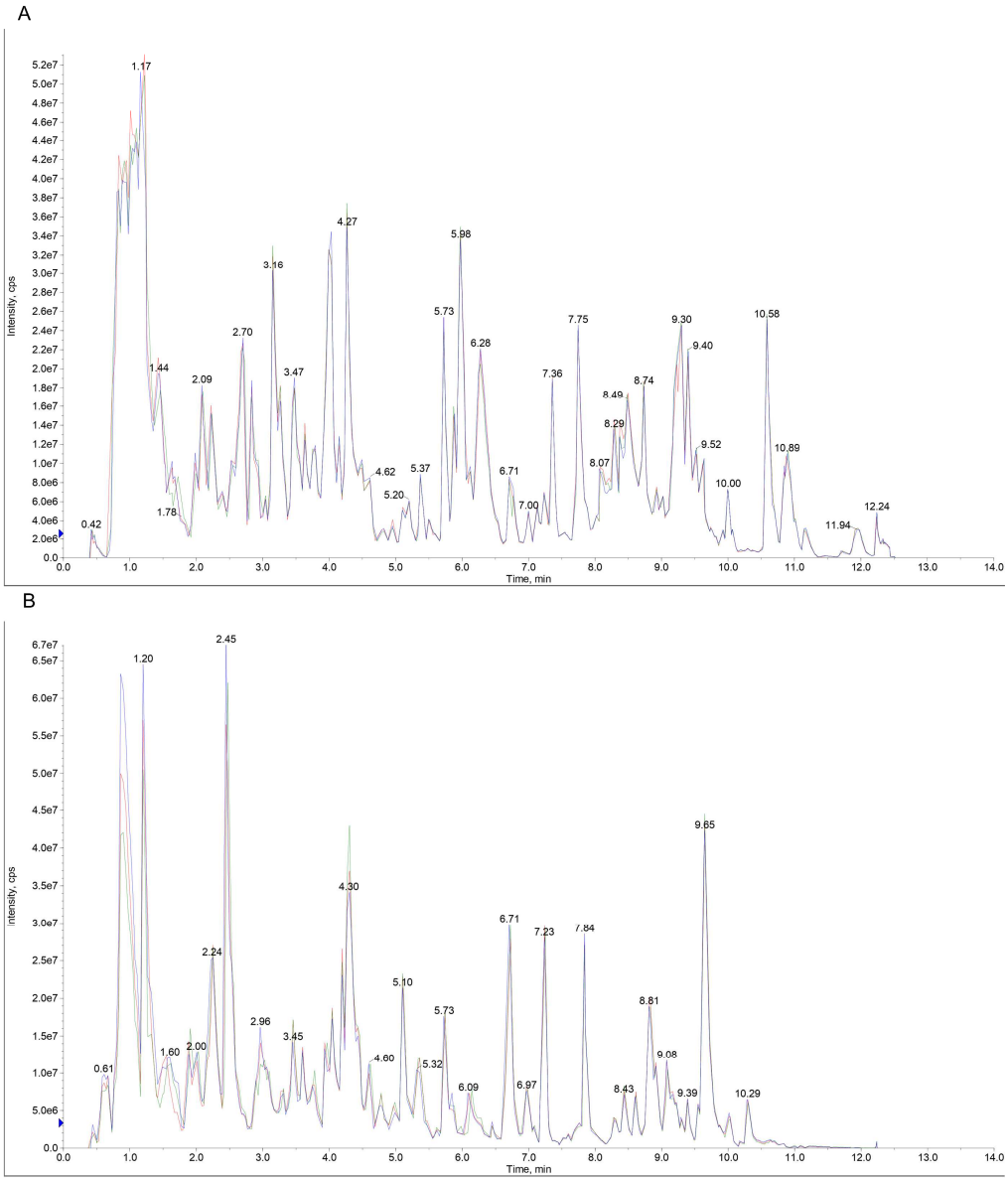

Fig. 2: Overlay plot of total ion chromatogram (TIC) for QC Sample as determined by Mass Spectrometry Detection. (A) Negative ion scan. (B) positive ion scan.

Table 1: Top 10 components information of D–C–T–P–D network.

Name	Component	CAS	Degree	Database source
RY-W73	Emodin	518-82-1	84	SwissTargetPrediction/SymMap
RY-W70	Coumarin	91-64-5	73	SwissTargetPrediction/SymMap
RY-W67	Choline	62-49-7	73	SymMap
RY-W66	Catechin	154-23-4	66	TCMSP/SymMap
RY-W43	3-O-methyl quercetin	1486-70-0	53	SwissTargetPrediction/SymMap
RY-W57	7-Hydroxycoumarin; umbelliferone	93-35-6	36	SwissTargetPrediction/SymMap
RY-W72	Embelin	550-24-3	33	SwissTargetPrediction/SymMap
RY-W79	Geniposide	24512-63-8	32	SymMap
RY-W9	2,3-Dihydroxyolean-12-en-28-oic acid (2-hydroxyoleanolic acid)	26707-60-8	31	SwissTargetPrediction
RY-W10	2,3-Bihydroxyurs-12-en-28-oic acid (corosolic acid)	4547-24-4	31	SwissTargetPrediction

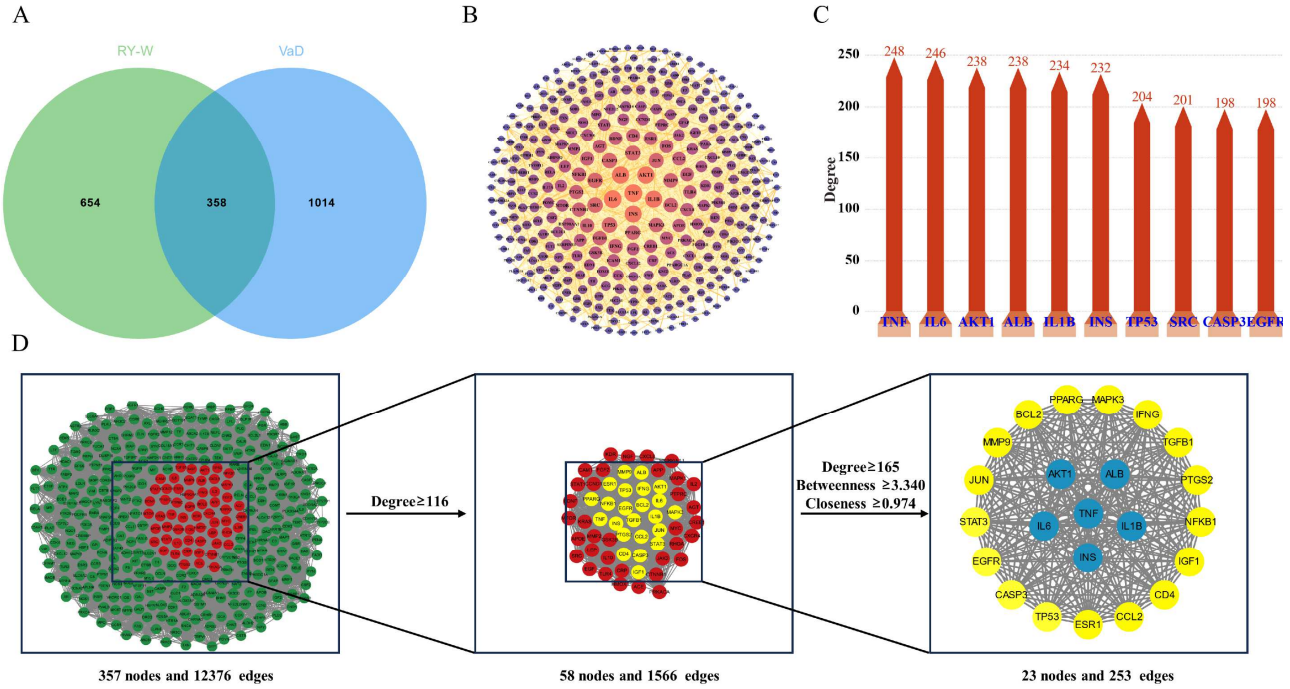

Fig. 3: Analysis of potential targets of action of *Rubia yunnanensis* water decoction (RY-W) for vascular dementia (VaD) treatment. (A) Venn diagram of potential targets of action of RY-W in VaD treatment. (B) PPI network of potential targets of RY-W. Circles represent target proteins. The larger the diameter of the circle and the brighter the color, the higher the degree value. Straight lines represent interactions between target proteins, and the thickness of the line represents the degree of interaction. (C) The top 10 targets with Degree values among the targets of VaD action for RY-W treatment. (D) Core targets screening process. Among the selected core targets, the targets with the top 6 Degree values are shown in blue, and other targets are shown in yellow. The thickness and color depth of the edges are proportional to the correlation between the targets.

Table 2: The binding energy of components and core target proteins (kcal/mol).

component/protein	AKT1	ALB	IL-1β	IL-6	INS	TNF
emodin	-6.7	-8.4	-6.8	-6.7	-6.0	-6.8
coumarin	-5.4	-6.9	-5.2	-5.4	-5.2	-6.5
choline	-3.2	-3.8	-3.2	-3.4	-2.8	-3.2
umbelliferone	-5.4	-7	-5.7	-5.4	-5.3	-6.6
embelin	-4.8	-6.7	-5.3	-5.5	-5.4	-5.1

RY-W D–C–T–P–D network analysis and key active components in VaD treatment

A D–C–T–P–D network was created to study the molecular mechanisms of RY-W in the therapy of VaD; Fig. 4C displays the collection of 510 nodes and 2366 lines. Each active constituent of RY-W-VaD corresponds to numerous targets and each target is connected with various pathways. This indicates that the proposed mechanism of RY-W in treating VaD involves many components, multiple targets and multiple pathways. Subsequently, we evaluated the primary active components of RY-W for the management of VaD by analyzing the degree centrality values (from network topology analysis) of the components in the D–C–T–P–D network. Emodin, coumarin, choline, catechin, 3-O methyl quercetin, 7-hydroxycoumarin, embelin, geniposide, 2,3-dihydroxyolean-12-en-28-oic acid (2-hydroxyoleanolic acid) and 2,3-dihydroxyurs-12-en-28-oic acid (corosolic acid) were the first 10 major components of RY-W (Table 1). This suggests that these RY-W major components may act on important targets of RY-W-VaD and thus influence the core pathways for treating VaD. It has been reported that ubiquitous interferences such as quercetin and catechin can lead to false-positive reports of biological activity (Pohjala & Tammela, 2012). Therefore, we screened the top five key active components by excluding polyphenolic false-positive components (e.g., quercetin, catechin) from the top 10 major components, finally identifying emodin, coumarin, choline, umbelliferone and embelin-all with Degree ≥ 33 (Degree values of 84, 73, 73, 36 and 33, respectively).

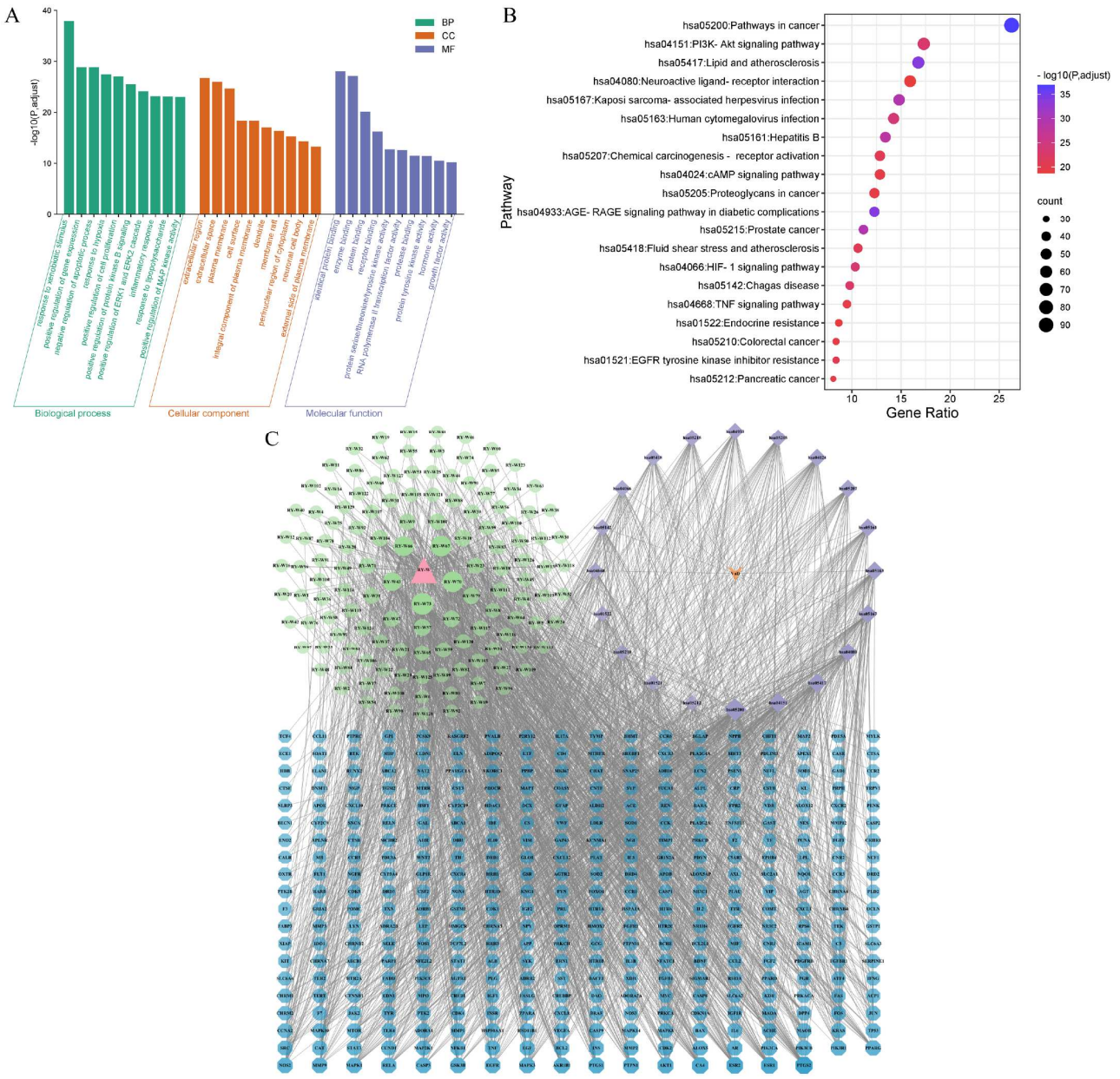

Fig. 4: GO and KEGG analyses, and D–C–T–P–D network. (A) The top 10 significantly enriched biological processes, cellular components and molecular functions in GO analysis were selected. x-axis indicates the enrichment score. (B) Selection of the top 20 significantly enriched pathways ($p < 0.05$). x-axis indicates the enrichment score. Red circles represent higher enrichment for a given KEGG pathway. (C) D–C–T–P–D network. Pink triangles represent *Rubia yunnanensis* water decoction (RY-W); green circles represent the active components of RY-W; orange V angle represents vascular dementia (VaD); purple diamonds represent the top 20 significantly enriched pathways; and blue octagons represent RY-W–VaD targets. The size and transparency of the nodes are proportional to the degree value.

Molecular docking analysis

The network pharmacology data were used to perform molecular docking in order to confirm the binding modalities of the top five active components of RY-W (emodin, coumarin, choline, umbelliferone and embelin) to the six core targets of RY-W-VaD (TNF, IL-6, ALB, AKT1, IL-1β and INS). According to table 2, these components bind to these proteins with different affinity. All components, except choline, had good binding affinities (binding energies <–5.0 kcal/mol except for one -4.8 kcal/mol) to the six core targets. Among them, emodin, umbelliferone and coumarin showed the strongest binding affinities with ALB, which were –8.4, –7.0 and –6.9, respectively. 2D and 3D visualization results of molecular docking for the top three molecules in terms of binding affinity are shown in fig. 4.

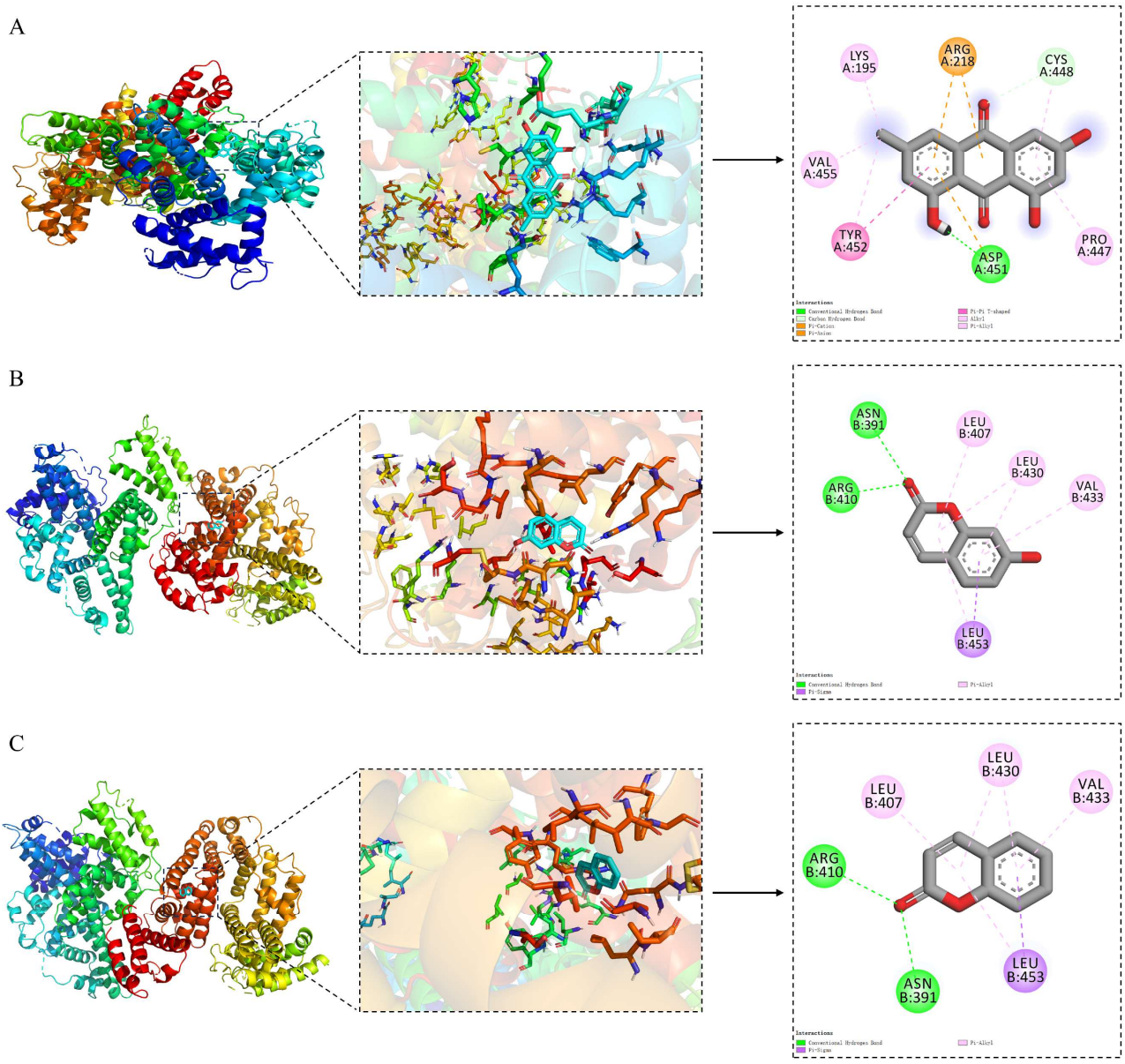

Fig. 5: Visualization of molecular docking for the top three molecules in terms of binding affinity. (A) 2D and 3D images of albumin (ALB)-emodin interaction surface and molecular docking results. (B) 2D and 3D images of ALB-umbelliferone interaction surface and molecular docking results. (C) 2D and 3D images of ALB- coumarin interaction surface and molecular docking results.

In ALB, emodin (Fig. 5A) formed hydrogen bonding interactions with ASP-451 and CYS-448, alkyl and Pi-alkyl hydrophobic interactions with LYS-195, VAL-455 and PRO-447, Pi-sulfur interactions with ARG-218 and Pi-Pi T-shaped interactions with TYR-452; umbelliferone (Fig. 5B) formed hydrogen bonding interactions with ASN-391 and ARG-410, a Pi-alkyl hydrophobic interactions with LEU-407, LEU-430, VAL-433 and LEU-453, a Pi-sigma interaction with LEU-453; coumarin (Fig. 5C) formed hydrogen bonding interactions with ASN-391 and ARG-410, a Pi-alkyl hydrophobic interactions with LEU-407, LEU-430, VAL-433 and LEU-453, a Pi-sigma interaction with LEU-453.

Molecular dynamics simulation results

Analysis of the 100 ns MD trajectory (Fig. 6) showed the albumin (ALB)-emodin complex's RMSD stabilized after 30 ns; the 30–100 ns trajectory was used for subsequent sampling. 100 conformations exhibited good superposition, with emodin stably binding to ALB's active site. RMSF and B-factor analyses revealed ALB had low overall flexibility (mostly < 2.0 A), with greater stability at the binding site; most emodin atoms were stable (RMSF < 2.0 A), except slight flexibility at the right cavity exterior. Ser 366, Arg 372, etc., mediated binding via water bridges and hydrogen bonds.

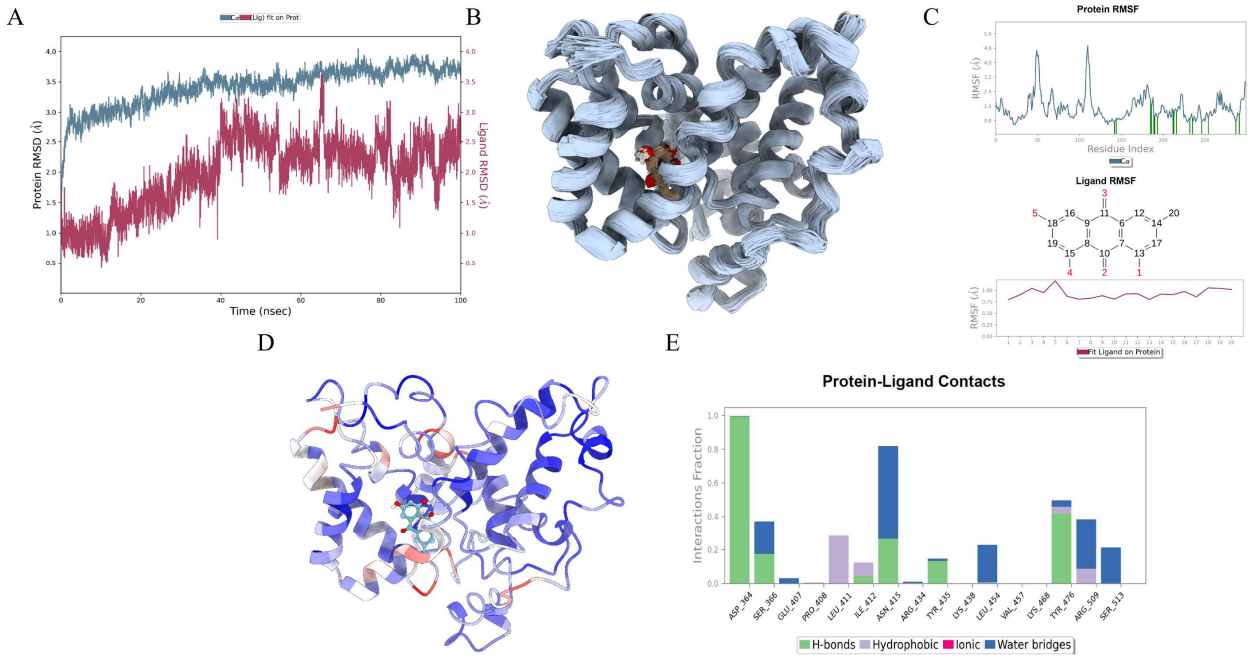

Fig. 6: Molecular dynamics simulation plots of albumin (ALB)-emodin complex. (A) RMSD of ALB-emodin (protein: blue, small molecule/emodin: red). (B) Superposition of 100 conformations from ALB-emodin's 100 ns simulation. (C) RMSF of ALB-emodin. (D) B-factor of ALB-emodin (blue: small RMSF, lower flexibility, higher stability; red: large RMSF, higher flexibility, lower stability). (E) Contribution of binding-site amino acids to emodin binding in ALB-emodin.

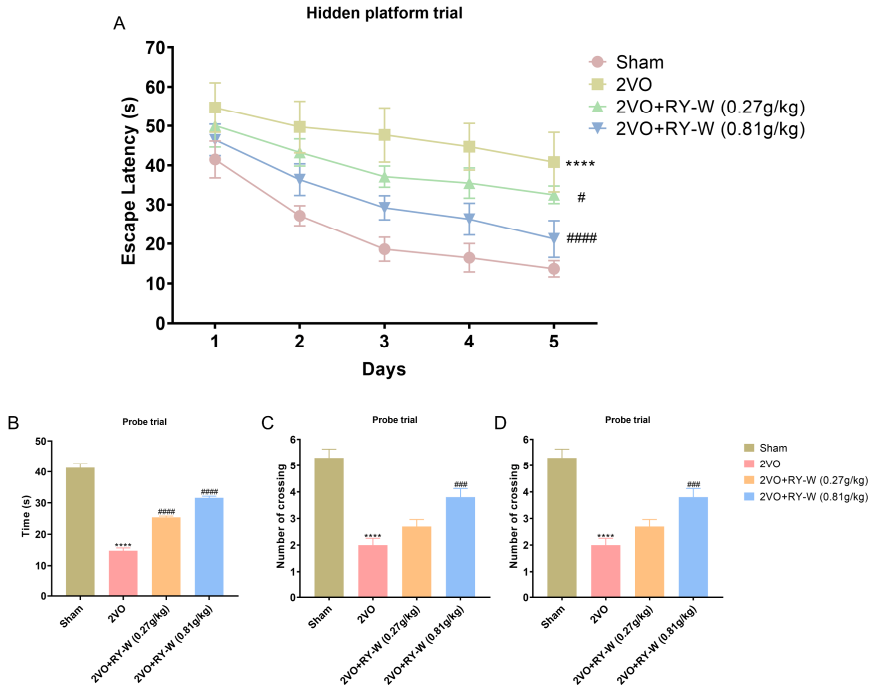

Fig. 7: *Rubia yunnanensis* water decoction (RY-W) administration improves learning and memory ability of vascular dementia (VaD) rats in the Morris water maze (MWM) test. (A) Mean escape latency of each group in the hidden platform trial. (B) Swimming duration of each group in the original platform quadrant during the probe trial. (C) Number of original platform crossings by each group in the probe trial. (D) Swimming speed of each group in the original platform quadrant during the probe trial. Data are expressed as mean ± SEM (n = 10). Compared with the Sham group, $^{****}p < 0.0001$; compared with the two-vessel occlusion (2VO) group, $^{\#}p < 0.05$, $^{\#\#\#}p < 0.001$, $^{\#\#\#\#}p < 0.0001$.

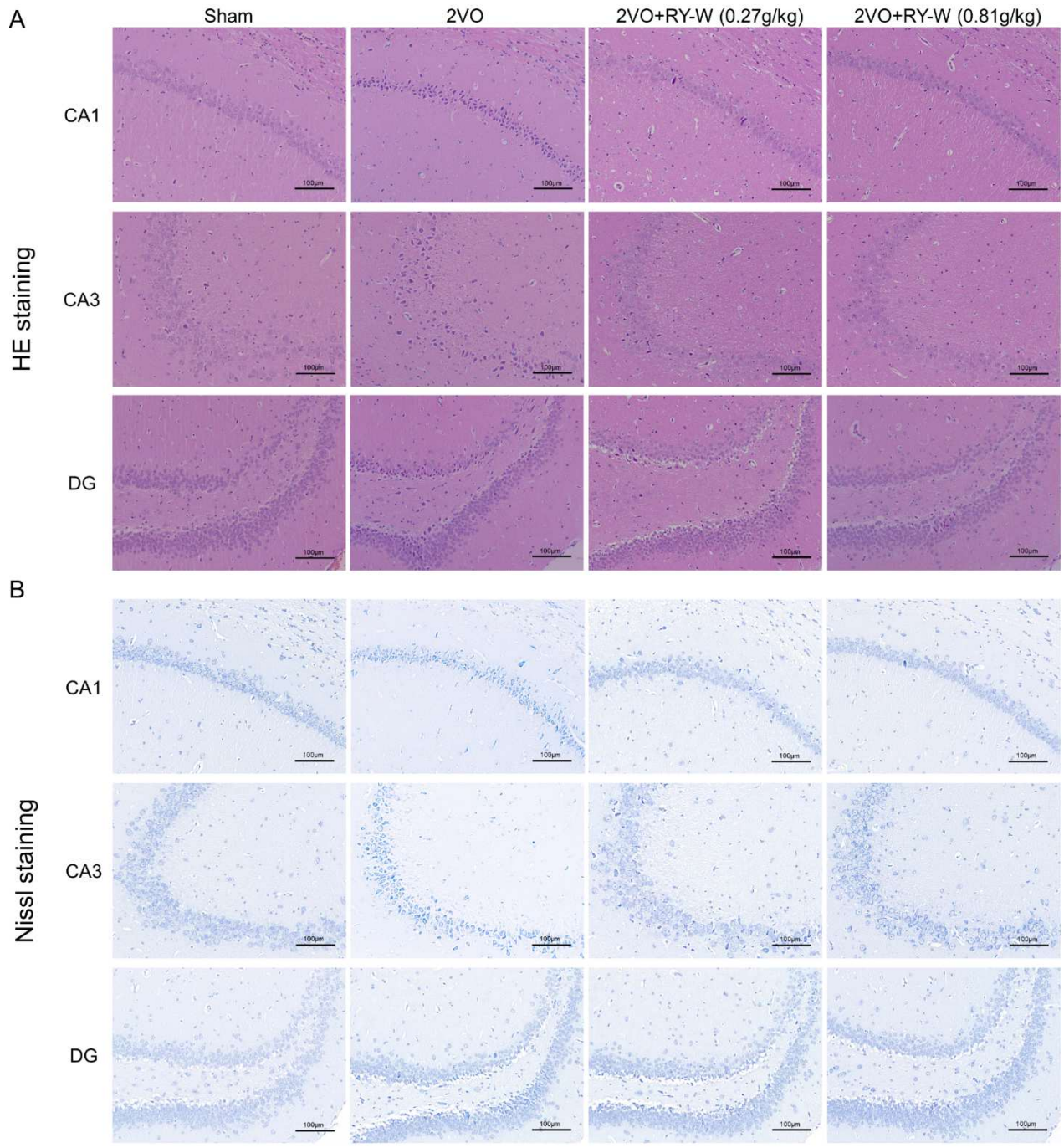

Fig. 8: Effects of *Rubia yunnanensis* water decoction (RY-W) administration on the morphology of neurons in CA1, CA3, and DG regions of the hippocampus of VaD rats (200 ×, n = 6). (A) Effect of hematoxylin and eosin (HE) staining on neuronal morphology in CA1, CA3 and DG regions of hippocampus of VaD rats. (B) Effect of Nissl staining on neuronal morphology in CA1, CA3 and DG regions of hippocampus of VaD rats.

Studies in biological systems

Learning and memory capacity are improved in VaD rats after RY-W administration

VaD is typically characterized by impaired spatial memory. The MWM test was used to assess if RY-W may enhance cognitive function in VaD rats (Yuan *et al*., 2019). The MWM test, comprising the hidden platform trial and probe trial, was employed to evaluate spatial learning and memory in a rat model of VaD. As illustrated in fig. 7A, the hidden platform trial revealed dynamic changes in escape latency across a 5-day training period. The escape latency was 23.46 ± 5.04 s in the Sham group, but significantly prolonged to 47.51 ± 2.35 s in the 2VO group (change: -24.05 s, 95% CI: -31.64 to -16.47 s, $p < 0.0001$).

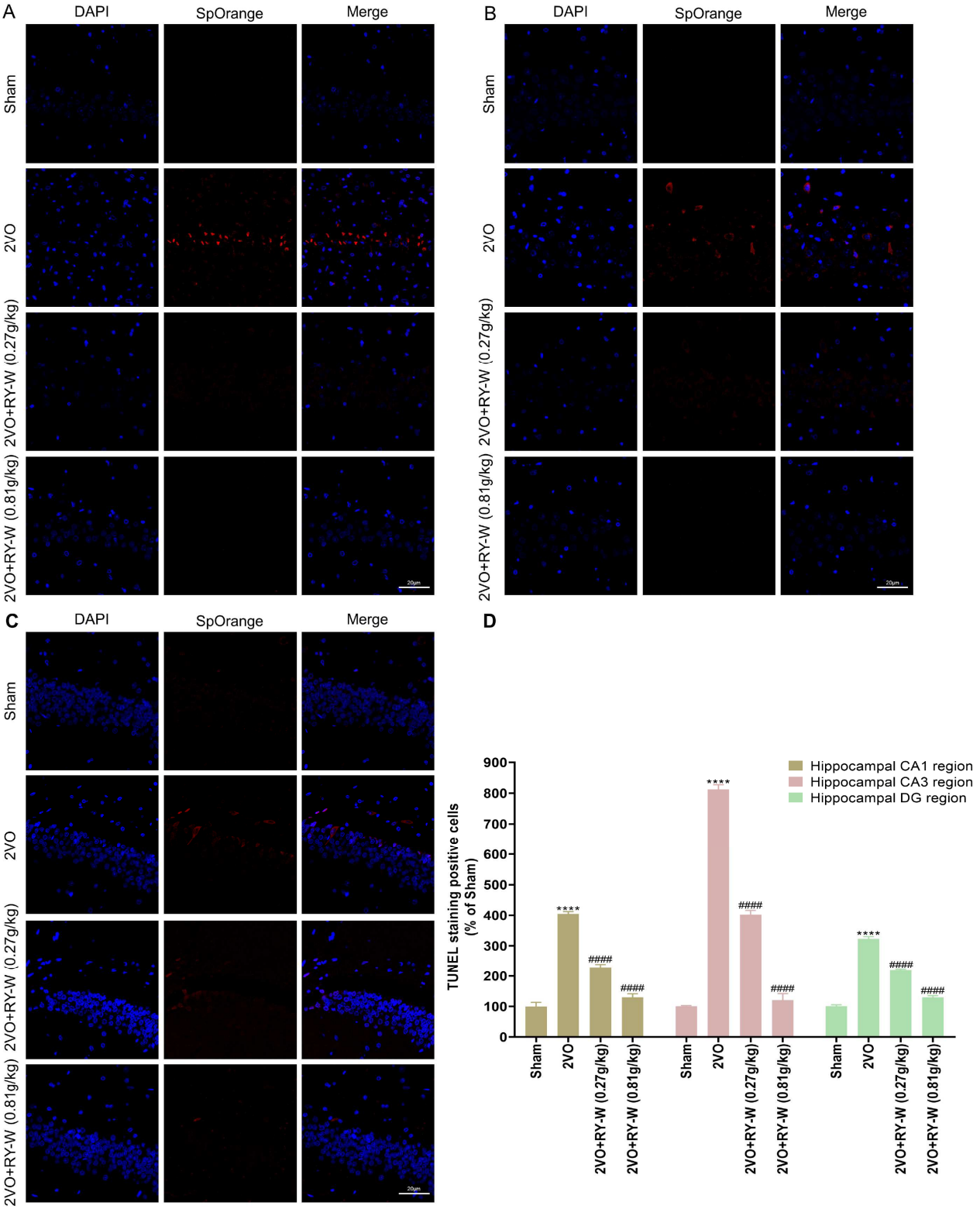

Fig. 9: Effect of *Rubia yunnanensis* water decoction (RY-W) administration on neuronal cell apoptosis in CA1 region (A) CA3 region (B) and DG region (C) of hippocampal tissue of vascular dementia (VaD) rats (400 ×). (D) quantitative analysis of the mean immunofluorescence intensity of neuronal cells in the three regions of hippocampal tissue. Data are expressed as mean ± SEM (n = 3). Compared with the Sham group, $^{****}p < 0.0001$; compared with the two-vessel occlusion (2VO) group, $^{\#\#\#\#}p < 0.0001$.

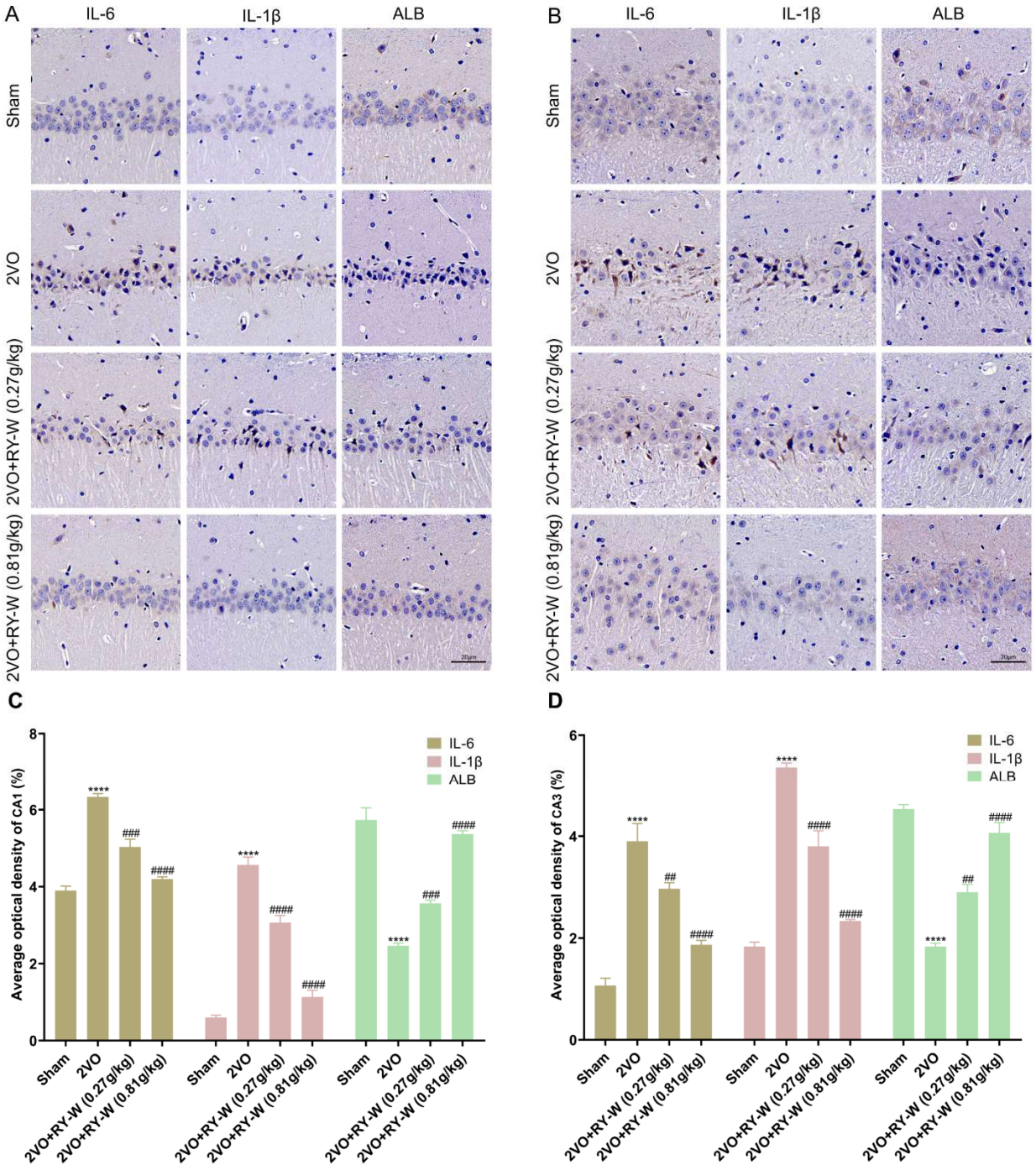

Fig. 10: Immunohistochemistry (IHC) staining of IL-6, IL-1β and albumin (ALB) in hippocampal tissue of vascular dementia (VaD) rats (400 ×). (A) Representative images of IL6, IL-1β, and ALB staining in each group of hippocampal CA1 region. (B) Representative images of IL6, IL-1β, and ALB staining for each group in the CA3 region of the hippocampus. (C-E) Quantitative analysis of IL-6, IL-1β, and ALB positive areas in CA1 and CA3 regions of each group. Data are expressed as mean ± SEM (n = 3). Compared with the Sham group, $^{****}p < 0.0001$; compared with the two-vessel occlusion (2VO) group, $^{\#\#}p < 0.01$, $^{\#\#\#}p < 0.001$, $^{\#\#\#\#}p < 0.0001$.

After RY-W treatment, it shortened to 39.68 ± 3.14 s in the low-dose group (0.27 g/kg; change vs. 2VO: 7.835 s, 95% CI: 0.250 to 15.42 s, $p = 0.0400$) and further to 31.89 ± 4.38 s in the high-dose group (0.81 g/kg; change vs. 2VO: 15.62 s, 95% CI: 8.04 to 23.21 s, $p < 0.0001$). A significant difference was also observed between the two dose groups (change: 7.79 s, 95% CI: 0.20 to 15.37 s, $p = 0.0417$), indicating RY-W improved spatial learning in VaD rats dose-dependently.

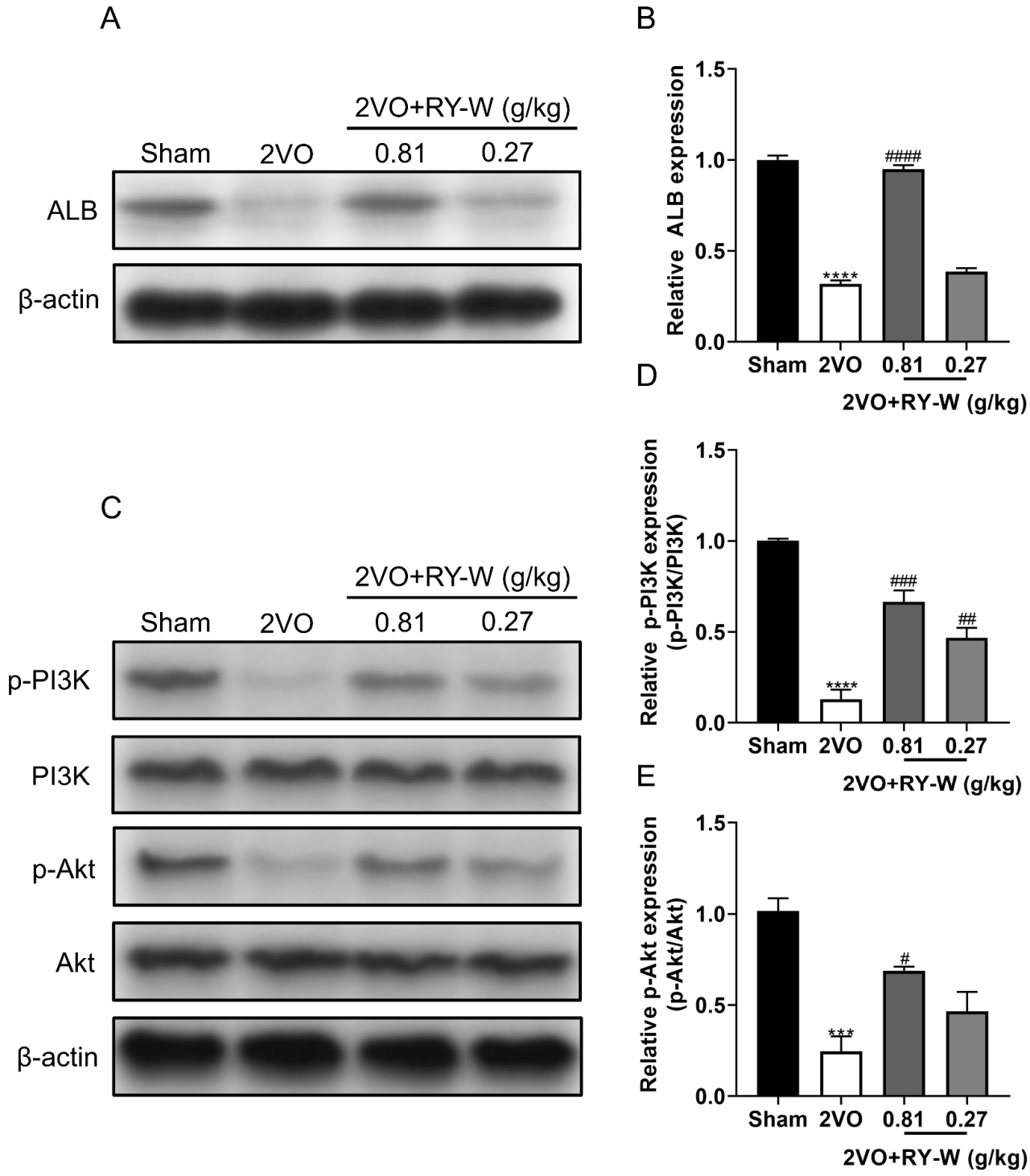

Fig. 11: Effect of *Rubia yunnanensis* water decoction (RY-W) on protein expression of albumin (ALB) and PI3K/Akt pathway in hippocampal tissues of vascular dementia (VaD) rats. Western blotting (WB) was performed to detect the expression of (A, B) ALB, (C, D) p-PI3K, and (C, E) p-Akt in hippocampal tissues of VaD rats. Results are expressed as mean ± SEM (n = 3). Compared with the Sham group, $^{***}p < 0.001$, $^{****}p < 0.0001$; Compared with the two-vessel occlusion (2VO) group, $^{\#}p < 0.05$, $^{\#\#}p < 0.01$, $^{\#\#\#}p < 0.001$, $^{\#\#\#\#}p < 0.0001$.

In the probe trial (Fig. 7B, C), spatial memory retention was assessed by analyzing quadrant preference and platform crossing frequency. Rats in the 2VO group spent significantly less time in the target quadrant (original platform location) and crossed the platform area fewer times than Sham rats (both $p < 0.0001$), indicating persistent memory dysfunction. Conversely, RY-W-treated rats displayed normalized behavioral patterns: the

0.81 g/kg RY-W group exhibited a marked increase in both target quadrant dwell time ($p < 0.0001$) and platform crossing frequency ($p < 0.001$). Notably, no evasive behaviors (e.g., floating, stagnation) were observed in any group and we further confirmed that swim speeds were comparable across all groups (Fig. 7D, $p > 0.05$) - together ruling out insufficient motivation or motor dysfunction as a confounder. These findings collectively demonstrate that RY-W administration ameliorates cognitive deficits in VaD rats by enhancing spatial learning acquisition and long-term memory retention.

RY-W improves neuronal morphology in rat hippocampal CA1, CA3 and dentate gyrus (DG) regions

Histological analysis is a crucial measure of nerve cell injury and the impact of drugs (Brun & Englund, 1986). Abnormalities in hippocampal neurons are associated with spatial memory and learning disabilities. Therefore, HE staining and Nissl staining were employed to examine the depletion of hippocampal neurons in the brain tissue of rats following modeling, as well as the extent of restoration after RY-W therapy. Fig. 8 demonstrates that the hippocampus neurons in the 2VO group exhibited considerable reduction compared to the Sham group. Additionally, the cell gap was enlarged, the cell count was reduced and the cell layout was chaotic. The above pathological changes were significantly attenuated by RY-W treatment. The trend of the results of HE staining and Nissl staining was consistent. We found that RY-W attenuated VaD-induced tissue damage, which was compatible with the results of the behavioral trials.

RY-W significantly attenuates neural cell apoptosis in rat hippocampal tissue

When apoptosis occurs, chromosomal DNA breaks and produces a large amount of sticky 3'-OH, which can form a chromogenic color with fluorescein at DNA nucleotide translocase, DNA nucleotides, etc. However, normal cell DNA remains unbroken, so it is rarely stained. In this investigation, we employed Tunel staining to identify neuronal apoptosis in the hippocampus region of the brain (Fig. 9). The results showed a significant increase in Tunel-positive cells and a significant elevation of apoptosis in the 2VO group compared to the Sham group ($p < 0.0001$). Compared with the 2VO group, RY-W treatment (0.27, 0.81 g/kg) led to a dramatic decrease in Tunel-positive cells and significantly inhibited apoptosis ($p < 0.0001$).

IHC analysis

The primary objectives of RY-W in the management of VaD, namely IL-6, IL-1B (a.k.a. IL-1β) and ALB, were chosen according to the network pharmacology's findings. These inflammatory markers were then examined in hippocampus tissues using IHC. Compared with the Sham group, IL-6 and IL-1β were significantly elevated and ALB was significantly reduced in the VaD rats' hippocampus tissue's CA1 and CA3 areas. In contrast, RY-W treatment effectively reduced IL-6 and IL-1β while elevating ALB, indicating that RY-W had a strong inhibitory effect on hippocampal neuronal inflammation in VaD rats (Fig. 10 A, B). Quantitative analysis performed by ImageJ yielded a more intuitive bar chart of the content of the three proteins in each group (Fig. 10 C, D). These results suggest that RY-W has a molecular mechanism to reduce inflammation and promote serum ALB production. The most pronounced impact was observed in the RY-W high-dose group (2VO + 0.81 g/kg RY-W).

WB analysis

The PI3K-Akt signaling pathway was identified as the most important route in the KEGG signaling pathway enrichment study, which is strongly associated with VaD. In addition, serum ALB is an important predictor of the risk of death from cerebrovascular disease and the amount of ALB expression is favorably associated with cognitive function (Gao *et al*., 2024; X. Yang *et al*., 2020). Therefore, in the present study, WB was used to detect the expression of ALB protein as well as the main proteins of the PI3K-Akt signaling pathway, PI3K, p-PI3K, Akt and p-Akt in hippocampal tissues. WB results showed that ALB (Sham: 1.000 ± 0.0239, 2VO: 0.3183 ± 0.0201, $p < 0.0001$; 0.81g/kg: 0.9486 ± 0.0233, $p < 0.0001$ vs 2VO), p-PI3K (Sham: 1.002 ± 0.0103, 2VO: 0.1302 ± 0.0517, $p < 0.0001$; 0.81g/kg: 0.6645 ± 0.0634, $p = 0.0003$ vs 2VO) and p-Akt (Sham: 1.016 ± 0.0700, 2VO: 0.2465 ± 0.0813, $p = 0.0005$; 0.81g/kg: 0.6877 ± 0.0235, $p = 0.0150$ vs 2VO) were significantly downregulated in 2VO-established VaD rats compared with the Sham group. In contrast, RY-W treatment significantly enhanced ALB and attenuated the inhibitory effect on p-PI3K/p-Akt in a dose-dependent manner (Fig. 11 A–E). These findings indicate that RY-W has the potential to ameliorate vascular dementia caused by chronic cerebral under-perfusion by activating ALB protein expression and promoting phosphorylation of the PI3K-Akt signaling pathway.

DISCUSSION

Our study reports that *Rubia yunnanensis* has a protective effect on brain nerve cells; thus, its role in central nervous system-related diseases can no longer be ignored (Cheng *et al*., 2024). In *ApoE*$^{-/-}$ mice given a high-fat diet for 12 weeks, the ethanol extract of *Rubia yunnanensis* increases p-PI3K/PI3K and p-Akt/Akt levels and decreases lipid levels, endothelial damage and carotid artery lipid buildup. (Li *et al*., 2024). Furthermore, it was shown that the methanol extract and ethyl acetate fraction of *Rubia yunnanensis* could effectively reduce triglyceride accumulation in HepG2 cells and olive oil mice, in which its chemical components, arborvane-type triterpenoids and free anthraquinone, were the effective lipid-lowering components (Gao *et al*., 2014). In addition, it is well known that lipid accumulation is one of the most critical pathologic factors in VaD (Dai *et al*., 2023); however, there

are no studies that have identified the direct effectiveness of RY-W in VaD and its mechanism of action. Multiple components of TCM can target multiple factors of the disease (Tao *et al*., 2020). Direct administration of RY-W from Yunnan is important to explore its mechanism in the treatment of VaD. Therefore, this study utilized network pharmacology, molecular docking and experimental validation to uncover the probable involvement of RY-W in VaD and its related molecular mechanisms.

This study is the first to comprehensively examine the mechanism of RY-W in curing VaD via a network pharmacology method. The use of LC and MS coupled with the TCM database search complemented each other, which avoided the homogeneity caused by using database search alone (Chu *et al*., 2016). In the current investigation, 1118 RY-W components in total, comprising 121 amino acids and their derivatives, 167 phenolic acids, 53 nucleotides and their derivatives, 105 flavonoids, 45 quinones, 81 lignans and coumarins, one ellagitannin, 113 alkaloids, 52 terpenes, 70 organic acids, one steroid, 157 lipids and 152 other classes, were described by use of the UPLC-MS/MS technique (Supplementary table 1). All the chemicals identified for RY-W were searched in three TCM databases, TCMSP, SwissDrugDesign and SymMap and screening yielded 154 active components and 1012 targets of RY-W (Supplementary table 2). With the help of four disease databases, DisGeNET, SymMap, TTD and GeneCards, 1372 VaD-related targets were obtained following the removal of duplicates (Supplementary table 3). In the next step, 358 potential targets of RY-W for the therapeutic management of VaD, i.e., the intersection targets of RY-W and VaD, were screened to construct the PPI network, in which the top six core targets (TNF, IL-6, ALB, AKT1, IL-1β and INS) with the highest degree values were finally identified. The D–C–T–P–D network of RY-W for VaD was also constructed and it was found that the top five key active components, emodin, coumarin, choline, umbelliferone and embelin had a higher number of therapeutic targets for VaD. Moreover, molecular docking demonstrated that the top five key active components of RY-W had a strong affinity for the top six core targets. Following this computerized computational phase of molecular docking, we constructed VaD model rats to evaluate the effectiveness of RY-W in treating learning and memory deficiencies in living organisms, applying different doses of RY-W for the intervention. These experiments showed that, based on the outcomes of the MWM test, 0.81 g/kg of RY-W reduced the time required to reach the hidden platform in VaD rats, suggesting that it had a substantial impact on improving memory functions. Finally, the core proteins and signaling pathways predicted by network pharmacology for RY-W against VaD were validated by WB and IHC analysis, confirming that it indeed plays a key role in the living rat model.

After analyzing the network topology, 23 of these gene targets, including TNF, IL-6, ALB, AKT1, IL-1β, INS, TP53, SRC, EGFR, CASP3, STAT3, JUN, MMP9, BCL2, PPARG, MAPK3, IFNG, TGFB1, IL-10, CTNNB1, PTGS2, NFKB1 and IGF1, were considered as candidate targets for RY-W in the prevention and treatment of VaD; there is an intricate relationship between these targets, forming a core PPI network. Among them, TNF, IL-6, ALB, AKT1, IL-1β and INS, which are ranked in the top six by degree value, are considered to be the core targets of RY-W for the prevention and treatment of VaD. TNF is a pro-inflammatory factor secreted by macrophages with two main types, TNF-α and TNF-β. Whereas neuroinflammation is a key factor in VaD, it has been widely reported that generalized pro-inflammatory factor levels are elevated in VaD (Belkhelfa *et al*., 2018). (2022) showed that naringenin improved cognitive impairment by decreasing the levels of pro-inflammatory factors (IL-1β, IL-6 and TNF-α) and increasing the levels of anti-inflammatory factors (IL-10 and IL-4). This mechanism resulted in the suppression of the inflammatory response in the hippocampus area of rats with vascular dementia. IL-6 is an immunomodulatory factor that is a key component of the immediate inflammatory reaction and has significant functions in both the central nervous system and immune system, including the maturation, activation, proliferation and immunomodulation of immune cells (Tanaka *et al*., 2014). (2022) showed that IL-6 is an inflammatory marker for the assessment of VaD and that higher IL-6 levels are correlated with a higher incidence of VaD. ALB, a water-soluble and abundant plasma protein, is synthesized by the liver, undertakes the binding and transport of exogenous drugs and is an important predictor of mortality risk in cerebrovascular disease (X. Yang *et al*., 2020). A prospective cohort study of 431,699 adults showed that there was a favorable correlation between the expression level of ALB and cognitive capacity (Gao *et al*., 2024). In addition, (2021) showed that trichostatin A could improve learning and memory behaviors in mice with the APP/PS1 genetic mutation by upregulating the expression level of ALB. Furthermore, ALB was negatively correlated with the neuroinflammatory responses of pro-inflammatory factors IL-6, IL-1β, TNF-α, etc (J. Li *et al*., 2022). AKT1 (serine and threonine kinase AKT) plays a crucial role as a protein in the PI3K-Akt signaling pathway, which promotes cell survival by regulating cell growth, division and inhibiting apoptosis (Gao *et al*., 2019). (2023) found that dulaglutide, a glucose-lowering drug, activated the PI3K-Akt-mTOR signaling pathway to alleviate learning memory deficits and neuronal damage in VaD rats. IL-1β is a cytokine that promotes inflammation and is generated and secreted by both immune and non-immune cells in response to inflammatory response signals. It can also synergize with TNF and IL-6 to induce VEGF production and contributes to angiogenesis. (2020) found that astaxanthin inhibited IL-1β expression and the MDA content to improve cognitive deficits in VaD mice. INS,

known as insulin, is a secreted protein that has the function of lowering blood glucose concentrations while accelerating the processes of glycolysis and glycogen synthesis. Epidemiologic studies have shown that individuals diagnosed with diabetes have a significantly elevated risk, ranging from 1.5 to 2 times greater, of developing dementia and cognitive impairment (Zhang *et al*., 2017). In addition, (2023) integrated transcriptomic and metabolomic studies also found that INS could effectively improve cognitive deficits in VaD rats by inhibiting astrocyte inflammation and neuronal apoptosis and downregulating tau and p-tau expression.

GO analysis indicated that the biological processes that may be involved in RY-W treatment of VaD mainly involve the response to xenobiotic stimulus, negative regulation of apoptotic processes, positive regulation of cell proliferation, inflammatory response and response to lipopolysaccharide. In VaD, RY-W preferentially affects the molecular function of identical protein binding, enzyme binding, receptor binding, etc. The results of GO analysis were mainly related to anti-inflammation, anti-apoptosis and lipid regulation.

KEGG pathway enrichment analysis revealed the underlying mechanism of RY-W in VaD may preferentially involve pathways in cancer, the PI3K-Akt signaling pathway, lipids and atherosclerosis, the TNF signaling pathway and fluid shear stress and atherosclerosis. Among them, the PI3K-Akt signaling pathway ranked second, involving 62 targets that contain IL-6, AKT1 and others involved in VaD. The PI3K-Akt signaling pathway is a well-established route that controls cell growth, metabolism and death, with functions including anti-inflammatory, antioxidant and neuroprotective. Activation of the regulation of this pathway plays a central role in the fight against VaD (Guan *et al*., 2023). PI3K phosphorylation acts as a second messenger to interact with Akt homologous proteins thereby activating phosphorylation. All phosphorylated Akt isoforms are highly expressed in all types of neuronal cells, exerting anti-apoptotic effects by promoting the expression of the downstream substrate mTOR. Furthermore, Akt inhibits GSK-3β phosphorylation at the Ser9 location, enhances neuronal viability and augments synaptic plasticity and also regulates learning and memory formation in VaD (Orike *et al*., 2001).

To assess the efficacy of RY-W in cognitive deficits, 2VO surgically replicated VaD rats were treated with RY-W via gavage for 1 month. In the MWM test, performed after the intervention, the inability of VaD rats to quickly find the hidden platform proved that the rats in this experiment were indeed impaired in spatial learning and memory. The results showed that the RY-W administration was effective in restoring cognitive deficits in these rats, proving its cognitive protective effect on 2VO surgically replicated VaD rats. Meanwhile, HE and Nissl staining intuitively demonstrated that RY-W administration could significantly inhibit neuronal cell death in the hippocampal CA1, CA3 and DG regions. Further analysis with the Tunel assay revealed that RY-W significantly inhibited apoptosis in hippocampal neurons, exerting an anti-apoptotic effect.

The WB results showed that treatment with RY-W stimulated the expression of p-PI3K and p-Akt in VaD rats, demonstrating that RY-W activates the PI3K-Akt pathway. The expression level of ALB protein was also significantly upregulated. IHC showed that treatment with RY-W significantly suppressed the expression levels of pro-inflammatory response factors and activated ALB in VaD rats. Experimental confirmation was provided for the predictions derived from network pharmacology. According to the above findings, this study suggests that RY-W can ameliorate cognitive deficits and neurological impairments in VaD by upregulating ALB expression and activating the PI3K-Akt pathway. Although the relevant results of this study partially revealed some of the therapeutic mechanisms of RY-W in the treatment of VaD, additional pharmacological experiments and methods are needed to validate other mechanisms predicted to be unnoticed in the analysis of our network pharmacological methods. These concerns will be resolved in future investigations. In addition, further studies of metabolite changes before and after RY-W administration may be needed to comprehensively understand the metabolic-related pathways via which RY-W ameliorates VaD.

CONCLUSION

In conclusion, RY-W exhibits protective effects in vascular dementia (VaD), the second most common form of dementia among the elderly and shows potential for the treatment of age-related neurodegenerative diseases. Our experiments showed that RY-W activated ALB expression and reduced the synthesis of pro-inflammatory factors (IL-6, IL-1β); it also activated the PI3K-Akt signaling pathway and these changes were associated with attenuated neuroinflammation, reduced neuronal apoptosis and improved cognitive deficits in VaD rats. The findings align with our forecasts based on network pharmacology and molecular docking. This research used a network pharmacology strategy to uncover the mechanism of RY-W in VaD. This is the first time that such a mechanism has been identified and it offers a theoretical foundation for using RY-W to treat VaD. Nevertheless, further pharmacological tests are still needed to investigate and clarify the molecular mechanisms of emodin, embelin, umbelliferone and coumarin the key chemical components of RY-W, in the treatment of VaD.

Acknowledgement
Not applicable.

Author's contributions

Conceptualization, J.C. and X.D.; methodology, J.C. and C.Z.; software, G.L.; validation, X.J. and L.Y.; formal analysis, J.C., G.L. and X.J.; investigation, J.C., P.C. and X.D.; resources, P.C. and X.D.; writing—original draft preparation, J.C.; writing—review and editing, X.J. and X.D.; visualization, J.C.; supervision, L.Y.; funding acquisition, C.Z. and X.D. All authors have read and agreed to the published version of the manuscript.

Funding

The present study was supported by the Xingdian Talent Support Program -Special for Young Talent (grant no. XDYC-QNRC-2022-0284), the High-level Talents Projects of Yunnan University of Chinese Medicine-Fifth Level Talents, the National Administration of Traditional Chinese Medicine High-Level Key Discipline Construction Project 'Minority Medicine (Dai Medicine)' (grant no. Zyyzdxk-2023193) and the Scientific Research Foundation of the Education Department of Yunnan Province (grant no. 2024Y372).

Data availability statement

The raw data presented in this study are contained in the supplementary data. Further inquiries may be addressed to the corresponding author.

Ethical approval

Animal welfare and experimental procedures follow the regulations of the ethics committee for animal research of Yunnan University of Chinese Medicine (Approval No. R-062022LH077).

Conflict of interest

The authors declare that there is no conflict of interest

REFERENCES

An X, Zhang Y, Duan L, Jin D, Zhao S, Zhou R, Duan Y, Lian F and Tong X (2021). The direct evidence and mechanism of traditional Chinese medicine treatment of COVID-19. *Biomed Pharmacother*, **137**: 111267.

Belkhelfa M, Beder N, Mouhoub D, Amri M, Hayet R, Tighilt N, Bakheti S, Laimouche S, Azzouz D, Belhadj R and Touil-Boukoffa C (2018). The involvement of neuroinflammation and necroptosis in the hippocampus during vascular dementia. *J Neuroimmunol*, **320**: 48-57.

Brun, A, & Englund, E. (1986). A white matter disorder in dementia of the Alzheimer type: A pathoanatomical study. *Ann Neurol*, **19**(3): 253-262.

Cheng J, Li G, Yang L, Chen P and Duan X (2024). Alcohol extract of Rubia yunnanensis: Metabolic alterations and preventive effects against OGD/R-induced oxidative damage in HT22 cells. *Biomed Rep*, **20**(5): 75.

Chu H, Tang Q, Huang H, Hao W and Wei X (2016). Grape-seed proanthocyanidins inhibit the lipopolysaccharide-induced inflammatory mediator expression in RAW264.7 macrophages by suppressing MAPK and NF-kappab signal pathways. *Environ Toxicol Pharmacol*, **41**: 159-166.

Collaborators GBDDF (2022). Estimation of the global prevalence of dementia in 2019 and forecasted prevalence in 2050: An analysis for the global burden of disease study 2019. *Lancet Public Health*, **7**(2): e105-e125.

Custodero C, Ciavarella A, Panza F, Gnocchi D, Lenato GM, Lee J, Mazzocca A, Sabba C and Solfrizzi V (2022). Role of inflammatory markers in the diagnosis of vascular contributions to cognitive impairment and dementia: A systematic review and meta-analysis. *Geroscience*, **44**(3): 1373-1392.

Dai J, Chan DKY, Chan RO, Hirani V, Xu YH and Braidy N (2023). The association between dietary patterns, plasma lipid profiles, and inflammatory potential in a vascular dementia cohort. *Aging Med (Milton)*, **6**(2): 155-162.

Fan F and Roman RJ (2021). Reversal of cerebral hypoperfusion: A novel therapeutic target for the treatment of AD/ADRD? *Geroscience*, **43**(2): 1065-1067.

Fraga CG, Clowers BH, Moore RJ and Zink EM (2010). Signature-discovery approach for sample matching of a nerve-agent precursor using liquid chromatography-mass spectrometry, XCMS, and chemometrics. *Anal Chem*, **82**(10): 4165-4173.

Gao PY, Ou YN, Wang HF, Wang ZB, Fu Y, He XY, Ma YH, Feng JF, Cheng W, Tan L and Yu JT (2024). Associations of liver dysfunction with incident dementia, cognition, and brain structure: A prospective cohort study of 431 699 adults. *J Neurochem*, **168**(1): 26-38.

Gao Y, Su Y, Huo Y, Mi J, Wang X, Wang Z, Liu Y and Zhang H (2014). Identification of antihyperlipidemic constituents from the roots of *Rubia yunnanensis* Diels. *J Ethnopharmacol*, **155**(2): 1315-1321.

Gao Y, Zhang M, Zhang R, You L, Li T and Liu RH (2019). Whole grain brown rice extrudate ameliorates the symptoms of diabetes by activating the IRS1/PI3K/AKT insulin pathway in db/db Mice. *J Agric Food Chem*, **67**(42): 11657-11664.

Guan T, Xiao Y, Xie X, Meng N, Qi Q, Xu J, Jiang X, Zhang Z, Teng Z and Lv P (2023). Dulaglutide improves gliosis and suppresses apoptosis/autophagy through the PI3K/Akt/mTOR signaling pathway in vascular dementia rats. *Neurochem Res*, **48**(5): 1561-1579.

Huang da W, Sherman BT and Lempicki RA (2009). Systematic and integrative analysis of large gene lists using DAVID bioinformatics resources. *Nat Protoc*, **4**(1): 44-57.

Huang P, Ke H, Qiu Y, Cai M, Qu J and Leng A (2019). Systematically characterizing chemical profile and potential mechanisms of qingre lidan decoction acting on cholelithiasis by integrating UHPLC-QTOF-MS and

network target analysis. *Evid Based Complement Alternat Med*, **2019**: 2675287.

Huang X, Zhang M, Song Y, Sun B, Lin L, Song X and Li C (2023). Integrated network pharmacology to investigate the mechanism of *Salvia miltiorrhiza* Bunge in the treatment of myocardial infarction. *J Cell Mol Med*, **27**(22): 3514-3525.

Li G, Cheng J, Yang L, Chen P and Duan X (2024). Ethanol extract of *Rubia yunnanensis* inhibits carotid atherosclerosis via the PI3K/AKT signaling pathway. *Biomed Rep*, **20**(2): 19.

Li J, Bai Y, Ma K, Ren Z, Li J, Zhang J and Shan A (2022). Dihydroartemisinin alleviates deoxynivalenol induced liver apoptosis and inflammation in piglets. *Ecotoxicol. Environ. Saf.*, **241**: 113811.

Li T, Zheng J, Wang Z, Xu L, Sun D, Song H, Wu S, Du M, Peng S and Zhang J (2022). Maresin 1 improves cognitive decline and ameliorates inflammation and blood-brain barrier damage in rats with chronic cerebral hypoperfusion. *Brain Res*, **1788**: 147936.

Liang CS, Li DJ, Yang FC, Tseng PT, Carvalho AF, Stubbs B, Thompson T, Mueller C, Shin JI, Radua J, Stewart R, Rajji TK, Tu YK, Chen TY, Yeh TC, Tsai CK, Yu CL, Pan CC and Chu CS (2021). Mortality rates in Alzheimer's disease and non-Alzheimer's dementias: A systematic review and meta-analysis. *Lancet Healthy Longev*, **2**(8): e479-e488.

Liang X, Li H and Li S (2014). A novel network pharmacology approach to analyse traditional herbal formulae: the Liu-Wei-Di-Huang pill as a case study. *Mol Biosyst*, **10**(5): 1014-1022.

Longa EZ, Weinstein PR, Carlson S and Cummins R (1989). Reversible middle cerebral artery occlusion without craniectomy in rats. *Stroke*, **20**(1): 84-91.

Meli R, Anighoro A, Bodkin MJ, Morris GM and Biggin PC (2021). Learning protein-ligand binding affinity with atomic environment vectors. *J Cheminform*, **13**(1): 59.

Morgan AE and Mc Auley MT (2024). Vascular dementia: From pathobiology to emerging perspectives. *Ageing Res Rev*, **96**: 102278.

Morris GM, Huey R, Lindstrom W, Sanner MF, Belew RK, Goodsell DS and Olson AJ (2009). AutoDock4 and AutoDockTools4: Automated docking with selective receptor flexibility. *J Comput Chem*, **30**(16): 2785-2791.

Mracsko E, Hugyecz M, Institoris A, Farkas E and Bari F (2010). Changes in pro-oxidant and antioxidant enzyme levels during cerebral hypoperfusion in rats. *Brain Res*, **1321**: 13-19.

Orike N, Middleton G, Borthwick E, Buchman V, Cowen T and Davies AM (2001). Role of PI 3-kinase, Akt and Bcl-2-related proteins in sustaining the survival of neurotrophic factor-independent adult sympathetic neurons. *J Cell Biol*, **154**(5): 995-1005.

Pan P, Ma Z, Zhang Z, Ling Z, Wang Y, Liu Q, Lin X, Xu P, Yang D, Zhi H, Wang R and Zhang X (2021). Acupuncture can regulate the peripheral immune cell spectrum and inflammatory environment of the vascular dementia rat, and improve the cognitive dysfunction of the rats. *Front Aging Neurosci*, **13**: 706834.

Pohjala L and Tammela P (2012). Aggregating behavior of phenolic compounds-A source of false bioassay results? *Molecules*, **17**(9): 10774-10790.

Qiang YX, Deng YT, Zhang YR, Wang HF, Zhang W, Dong Q, Feng JF, Cheng W and Yu JT (2023). Associations of blood cell indices and anemia with risk of incident dementia: A prospective cohort study of 313,448 participants. *Alzheimers Dement*, **19**(9): 3965-3976.

Shannon P, Markiel A, Ozier O, Baliga NS, Wang JT, Ramage D, Amin N, Schwikowski B and Ideker T (2003). Cytoscape: A software environment for integrated models of biomolecular interaction networks. *Genome Res*, **13**(11): 2498-2504.

Skrobot OA, Black SE, Chen C, DeCarli C, Erkinjuntti T, Ford GA, Kalaria RN, O'Brien J, Pantoni L, Pasquier F, Roman GC, Wallin A, Sachdev P, Skoog I, group V, Ben-Shlomo Y, Passmore AP, Love S and Kehoe PG (2018). Progress toward standardized diagnosis of vascular cognitive impairment: Guidelines from the vascular impairment of cognition classification consensus study. *Alzheimers Dement*, **14**(3): 280-292.

Su Q, Li T, He PF, Lu XC, Yu Q, Gao QC, Wang ZJ, Wu MN, Yang D and Qi JS (2021). Trichostatin A ameliorates Alzheimer's disease-related pathology and cognitive deficits by increasing albumin expression and Abeta clearance in APP/PS1 mice. *Alzheimers Res Ther*, **13**(1): 7.

Tanaka T, Narazaki M and Kishimoto T (2014). IL-6 in inflammation, immunity, and disease. *Cold Spring Harb Perspect Biol*, **6**(10): a016295.

Tang L, Wang Y, Gong X, Xiang J, Zhang Y, Xiang Q and Li J (2023). Integrated transcriptome and metabolome analysis to investigate the mechanism of intranasal insulin treatment in a rat model of vascular dementia. *Front Pharmacol*, **14**: 1182803.

Tao T, Liu M, Chen M, Luo Y, Wang C, Xu T, Jiang Y, Guo Y and Zhang JH (2020). Natural medicine in neuroprotection for ischemic stroke: Challenges and prospective. *Pharmacol Ther*, **216**: 107695.

Trott O and Olson AJ (2010). AutoDock Vina: Improving the speed and accuracy of docking with a new scoring function, efficient optimization, and multithreading. *J Comput Chem*, **31**(2): 455-461.

Wang J, Ma Q, Li Y, Li P, Wang M, Wang T, Wang C, Wang T and Zhao B (2020). Research progress on Traditional Chinese Medicine syndromes of diabetes mellitus. *Biomed Pharmacother*, **121**: 109565.

Wei C, Zhu Z, Zheng JN, Lu Y, Cao C, Qu S, Liu M, Meng XE, Lou Q, Wang Q, Duan JA, Shang EX, Han Z and Zhu Y (2022). Chinese medicine, succinum, ameliorates cognitive impairment of carotid artery ligation rats and inhibits apoptosis of HT22 hippocampal cells via regulation of the GSK3beta/beta-catenin pathway. *Front Pharmacol*, **13**: 867477.

Xiang Y, Guo Z, Zhu P, Chen J and Huang Y (2019). Traditional Chinese medicine as a cancer treatment: Modern perspectives of ancient but advanced science. *Cancer Med*, **8**(5): 1958-1975.

Yang H, Wang W, Jia L, Qin W, Hou T, Wu Q, Li H, Tian Y and Jia J (2020). The effect of chronic cerebral hypoperfusion on blood-brain barrier permeability in a transgenic Alzheimer's disease mouse model (PS1V97L). *J Alzheimers Dis*, **74**(1): 261-275.

Yang X, Wang L, Zheng L, Wu J, Liu J, Hao Z, Zhang S, Wu B, Liu M and Wang D (2020). Serum albumin as a potential predictor of pneumonia after an acute ischemic stroke. *Curr Neurovasc Res*, **17**(4): 385-393.

Yin YL, Liu YH, Zhu ML, Wang HH, Qiu Y, Wan GR and Li P (2022). Floralozone improves cognitive impairment in vascular dementia rats via regulation of TRPM2 and NMDAR signaling pathway. *Physiol Behav*, **249**: 113777.

Yuan Z, Zhou H, Zhou N, Dong D, Chu Y, Shen J, Han Y, Chu XP and Zhu K (2019). Dynamic evaluation indices in spatial learning and memory of rat vascular dementia in the morris water maze. *Sci Rep*, **9**(1): 7224.

Zhang J, Chen C, Hua S, Liao H, Wang M, Xiong Y and Cao F (2017). An updated meta-analysis of cohort studies: Diabetes and risk of Alzheimer's disease. *Diabetes Res Clin Pract*, **124**: 41-47.

Zhang J, Zhang Y, Liu Y and Niu X (2022). Naringenin attenuates cognitive impairment in a rat model of vascular dementia by inhibiting hippocampal oxidative stress and inflammatory response and promoting N-Methyl-D-aspartate receptor signaling pathway. *Neurochem Res*, **47**(11): 3402-3413.

Zhu N, Liang X, Zhang M, Yin X, Yang H, Zhi Y, Ying G, Zou J, Chen L, Yao X and Li H (2020). Astaxanthin protects cognitive function of vascular dementia. *Behav Brain Funct*, **16**(1): 10.